AFOSR-TR-96-0260

53.301-298 Standard Form 298, Report Documentation Page.

REPORT DOCUMENTATION PAGE

Form Approved
OMB No. 0704-0188

1. AGENCY USE ONLY (Leave blank)	2. REPORT DATE	3. REPORT TYPE AND DATES COVERED
	05/23/96	Final, 10/01/92 - 09/30/95

4. TITLE AND SUBTITLE
Thrust-Induced Effects on a Pitching-Up Delta Wing Flow Field

5. FUNDING NUMBERS
F49620-93-I-0013

6. AUTHOR(S)
L. Lourenco, C. Shih, L. van Dommelen & A. Krothapalli

7. PERFORMING ORGANIZATION NAME(S) AND ADDRESS(ES)
Dept. of Mechanical Engineering
Florida A&M University
2525 Pottsdamer St., Tallahassee, FL 32310

8. PERFORMING ORGANIZATION REPORT NUMBER
FMRL-TR96-1

9. SPONSORING/MONITORING AGENCY NAME(S) AND ADDRESS(ES)
Air Force Office of Scientific Research
Division of Aerospace Sciences
Bolling AFB, Washington DC 20332-6448

NA

10. SPONSORING/MONITORING AGENCY REPORT NUMBER
93-I-0013

11. SUPPLEMENTARY NOTES

12a. DISTRIBUTION/AVAILABILITY STATEMENT
Approved for public release,
distribution unlimited

13. ABSTRACT (Maximum 200 words)

Experimental study of thrust-induced effects on a pitching-up 60 deg. delta wing was conducted. A downward vectored trailing edge jet has a significant effect in delaying the vortex breakdown. Strong asymmetric vortex bursting can be induced using asymmetric jet control. Detailed PIV measurements are taken to characterize the vortex flow field with and without jet control. A parallel experiment of the vortex flow over a 75 deg. delta wing is made to further the understanding of the vortex breakdown phenomenon. Related investigations of dynamic stall phenomena over a pitching airfoil are also summarized. Concurrently, considerable efforts have been made in the development of an innovative computational scheme. A grid-free vortex distribution technique is introduced to simulate the diffusion process of a vortex-dominated flow. This allows the readily extension of the 2-D vortex method to be used in a 3-D flow field such as a pitching-up delta wing configuration. Several computational examples will be discussed.

14. SUBJECT TERMS	15. NUMBER OF PAGES
	38
	16. PRICE CODE

17. SECURITY CLASSIFICATION OF REPORT	18. SECURITY CLASSIFICATION OF THIS PAGE	19. SECURITY CLASSIFICATION OF ABSTRACT	20. LIMITATION OF ABSTRACT

DISCLAIMER NOTICE

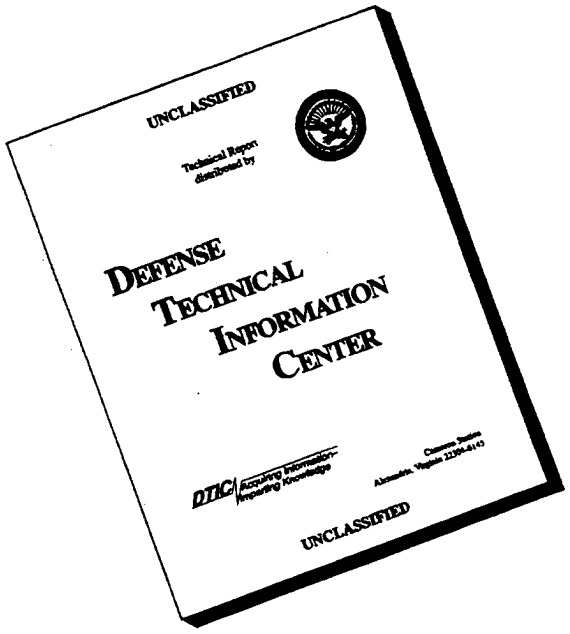

THIS DOCUMENT IS BEST QUALITY AVAILABLE. THE COPY FURNISHED TO DTIC CONTAINED A SIGNIFICANT NUMBER OF PAGES WHICH DO NOT REPRODUCE LEGIBLY.

Thrust-Induced Effects on a Pitching-Up Delta Wing Flow Field

by

L. Lourenco, C. Shih, L. Van Dommelen and A. Krothapalli

Department of Mechanical Engineering
FAMU/FSU College of Engineering
Florida A&M University and Florida State University
Tallahassee, Florida 32316-2175

Contract # F49620-93-I-0013

Prepared for

Air Force Office of Scientific Research
Bolling Air Force Base, Washington DC 20332
Final Report for the Period October 1, 1992 - September 30, 1995

Thrust-Induced Effects on a Pitching-Up Delta Wing Flow Field

L. Lourenco, C. Shih, L. van Dommelen and A. Krothapalli
Department of Mechanical Engineering
FAMU-FSU College of Engineering
Florida A&M University and Florida State University
Tallahassee, Florida 32310

Introduction

Experimental study of thrust-induced effects on a pitching-up 60° sweep angle delta wing was conducted in a water towing tank facility. The Reynolds number, based on the free stream velocity and the root chord, is 9,800. Both static and dynamic (pitching) conditions are tested. The wing is pitched from 10^{o} to 45^{o} angle of attack with pitch rates varied from 0.05 to 0.45. A downward vectored, trailing edge jet has a significant effect in delaying the vortex breakdown on a delta wing, under both static and dynamic pitching conditions. Strong asymmetric bursting of the leading edge vortices can be induced by arranging the vectored jet in an asymmetric configuration. Transient pitching motion has been shown to significantly delay the onset of vortex breakdown. Detailed PIV measurements are taken along both the cross stream plane and the vortex core plane of the leading edge vortices with or without the influence of the vectored jets. A parallel experiment of the vortex flow field over a 75° sweep angle delta wing is also undertaken to further the understanding of the vortex breakdown phenomenon. Related investigations of dynamic stall phenomena over a pitching up two-dimensional airfoil are also summarized.

Concurrently, considerable efforts have been made in the development of an innovative computational scheme. A grid-free vortex redistribution technique is introduced successfully to simulate the diffusion process of a vortex-dominated flow. This allows the readily extension of the two-dimensional vortex method to be used in a three-dimensional flow field such as a pitching-up delta wing. The computational study will be presented first.

1 Computational Research

Computational studies were conducted by Van Dommelen and by PhD students Szu-Chuan Wang and Shankar Subramaniam. The areas addressed are summarized below and described in more detail in the next subsections.

An investigation into manipulation of separating flows was conducted. It was found that the stall follows an unsteady separation process of the form discovered by Van Dommelen and Shen [11, 12]. It was also found that our results for the location of flow reversal agree with the predictions of unsteady thin airfoil theory, although some other results in literature do not. Suction is effective in preventing unsteady stall, and the computed scaled suction coefficients are similar to those for steady separation. Numerical experiments were also conducted on the effects of wall motion and small perturbations. The mechanics of stall was clarified through a separate local analysis of the leading edge region. A new approximate theory was developed to predict the occurrence of separation [25].

A second area addressed was the development of truly mesh-free Lagrangian methods. A method was developed in which the computational points are completely independent. The method has been advanced from the one-dimensional heat equation to separating flows with strong convection effects and to three-dimensional Stokes flows. This method eliminates the need for mesh generation completely, making it suitable to flows around complex configurations. Because there is no need to interpolate the vorticity onto a mesh or perform remeshing, false numerical diffusion is totally eliminated. The method has further no limits on the achievable order of accuracy, excellent conservation properties and can resolve very short scales [6, 7, 8, 9, 20, 23].

Significant advances were made in understanding the effects of an initial unsteady separation on the aerodynamic forces. A new formula to compute the drag was discovered which allows for higher accuracy. Using the new formula, the boundary layer evolution can directly be related to the drag. It was found that the initial effect of unsteady separation on the forces is small, making the problem of control nontrivial [22].

Another area addressed was the development of improved 3D Lagrangian procedures on regularly structured computational topologies. Most conventional factorization procedures for the 3D compressible Navier-Stokes equations are not stable in a Lagrangian computation. An ADI factorization was

developed in which the hyperbolic terms are grouped together in a bidiagonal discretization. This procedure has been tested in Lagrangian boundary layer computations and proved a significant advance over the existing procedures [18].

A further investigation was conducted into second order effects on unsteady separation. It was found that second order effects bring in significant short scale phenomena. The results indicate that the secondary eddies observed during unsteady separation do not indicate significant additional physics [21, 23].

1.1 Manipulation of separated flows

The issue of unsteady stall was addressed. Previous numerical results [10] showed that at high angles of attack, the first significant flow development is the occurrence of unsteady boundary layer separation. The separation is located near the leading edge and takes the form of a local thickening of the boundary layer according to a process discovered by Van Dommelen and Shen [11, 12]. By detailed studies of the flow near the leading edge, it was shown that this separation is distinct from the separation which develops near the trailing edge and which moves upstream from that location.

Other authors have reported trailing edge separations which would move upstream sufficiently far to reach the leading edge region. However, their definition of 'separation' was based on the streamline picture. It is known that in unsteady flow the streamline picture, including the formation of a 'recirculating wake' or a streamline leaving the wall does not imply a significant departure of most of the boundary layer fluid away from the wall.

Due to the actual separation process, commonly known as the Van Dommelen and Shen singularity, an extensive dynamic stall vortex develops above the wing. By numerically tracking the vorticity, it was shown conclusively that while this vortex moves downstream out of the leading edge region, the vorticity it contains does originate from the leading edge.

While the lift only collapses when the main vortex leaves the vicinity of the wing surface, experience shows that it is difficult to prevent this loss of wing effectiveness once the vortex has been shed from the leading edge. For that reason, recent work has focussed on eliminating the vortex altogether. To do that, the Van Dommelen and Shen process must be prevented. The structure of the Van Dommelen and Shen process [12] provides insight in

what procedures can be effective.

It is known that the process requires a layer of boundary layer fluid near the wall with vorticity of opposite sense compared to the remaining boundary layer above it. This reversed vorticity is ordinarily associated with reversed flow in the boundary layer. However, it is possible for the process to occur even after the reversed flow has been eliminated by a favorable pressure gradient. An effective procedure to prevent separation is to remove the reversed vorticity by means of suction through the wing surface. This renders the Van Dommelen and Shen process impossible. It is well known that suction is effective for steady separation, which forms the limiting case of unsteady separation.

Figure 1 shows that for a NACA 0012 airfoil large scale separation occurs. In this case, the airfoil was started impulsively at 30 degrees angle of attack. Applying a small amount of suction maintains the attached flow as shown. The computed scaled suction coefficients agree well with experimental values at much higher Reynolds numbers [25].

The Van Dommelen and Shen process takes a sizable time to develop, and one might wonder whether it is possible to reduce the amount of suction by starting late in the process. By a series of Navier Stokes simulations, we showed that this is indeed the case. Moreover, we found that when the angle of attack is reduced back to a small value, it is possible to stop suction early. The optimal application for suction was found to be suction distributed from the leading edge to about 20% of the chord. There is some existing experimental support for this result, as well as theoretical arguments in its favor. However, some others have argued that suction through a slit would be more effective. The nondimensional scaled suction coefficients we obtained agree with literature values at much higher Reynolds numbers, in the range of 10^6 [25].

Numerical experiments were also conducted on the use of wall motion to prevent separation. However, it was concluded that the wall motion required to prevent separation was unrealistically high. Experiments were also conducted on the influence of small perturbations on the Van Dommelen & Shen process. It is known that this process is highly sensitive to small perturbations at high Reynolds numbers. However, the results are inconclusive. It seems that a higher Reynolds number is needed to address this issue.

An asymptotic numerical analysis of the leading edge region was conducted. In this model, the leading edge takes a parabolic shape. It shows

that flow reversal will normally form locally at the leading edge, and not propagate there from the trailing edge region. This agreed with our results for the full airfoil, but disagrees with some other results in literature.

An approximate method was devised to predict separation. According to the model, separation consists of two separate stages: (a) viscous retardation of the boundary layer fluid due to an adverse pressure gradient, resulting in flow reversal; (b) inviscid break-up due to local particle accumulation in the middle of the boundary layer. According to the model, the time scale for the first stage is given by the pressure gradients, while the second stage is determined by the changes in pressure gradient. The model compares well with exact solutions for the location of separation.

1.2 The redistribution method.

A new computational method has been developed that allows computation on arbitrarily located computational points [6, 7, 8, 9, 15, 16, 20, 23]. Figure 2 shows computational points when two point vortices in free space diffuse out. There is no structure to the point locations, yet our method allows accurate computation [9, 20]. Unlike unstructured computations, the method requires no partitioning of the domain, or any other mesh generation. The method itself takes care of creating new computational points where needed. It should therefor be suitable for highly complex three-dimensional domains, and for flows with strong convection effects.

We showed theoretically and exponentially that even for strong straining the computational point density is finite in the method, resulting in superior performance on short scale phenomena. We showed that there is no theoretical limit on the order of accuracy achievable with the method. The method also has excellent conservation properties, and reduces the numerical errors in the velocity field.

As a numerical example, we addressed the unsteady separation from a circular cylinder at a Reynolds number 9,500. This flow has proved to be a formidable challenge for recent finite difference, spectral, and vortex computations. Our method produced converged results at a small fraction of the number of computational points of any other computation. Our results agree with the other computations where these agree with one another, and our results seem more accurate where the other methods differ from one another.

Figure 3 shows the evolution of the vorticity field. Figure 4 show the

convergence of our vorticity field with time step. Note that all spatial computational scales are proportional to the square root of the time step. The figure shows that our vorticity field is converged.

Our results also agree very well with those of Koumoutsakos and Leonard [5]. Yet we used only a small fraction of the vortices of that computation. The results of Koumoutsakos and Leonard are in fact closest to our medium resolution results; this suggests that they may still have some numerical dissipation despite the larger number of vortices. The reason is believed to be the capability of our method to resolve finer scales with less points than particle-strength exchange methods.

Figure 5 compares the drag coefficients obtained by recent computations. Our results seem to be converged with mesh size. Note that there are noticeable discrepancies between the various other computations.

According to our results, the best other computation is a spectral element computation by Paul Fischer and G. W. Kruse. The spectral computation does not show the dip in the drag experienced by some other authors, but not by us. The spectral method used 6000 spectral elements for half the flow region, each element with 100 degrees of freedom. For comparison, our medium resolution computation, used only 63,000 vortices for the full flow region.

We have found experimentally that the drag is highly dependent on the exponentially small rotational velocity above the boundary layer, and that a very stringent cut-off of the vorticity is required to get converged results. This numerical difficulty was predicted analytically ten years ago by Van Dommelen & Shen [13] on basis of their analytical solution for the rear stagnation point. It is the most likely explanation of the difficulties experienced by some of the other authors.

Figure 6 compares the computed velocity profiles with boundary layer theory for an early time. The agreement is excellent. Furthermore, our Navier-Stokes computation follows the more accurate second order boundary layer theory where it differs from the plain boundary layer results.

Figure 7 shows our results for the drag at Reynolds numbers from 550 up to 40,000. This is the first time that accurate results at Reynolds numbers 20,000 and 40,000 have been obtained. Our results follow boundary layer theory as long as it remains accurate. The boundary layer results become inaccurate at a time depending on the Reynolds number, indicated by increasing deviations between first and second order boundary layer theory.

The results of Collins and Dennis [2], which are valid at small times, suggest that the Navier-Stokes solution should be in between the first and second order boundary layer theory. Our results confirm this. Furthermore, for increasing Reynolds number, the Navier-Stokes results should approach second order boundary layer theory more closely than first order theory. Our results confirm this. All these observations indicate that our Navier-Stokes results are indeed very accurate.

Figure 8 shows the vorticity evolution at Reynolds number 20,000. Figure 9 verifies the numerical convergence. According to Van Dommelen & Shen [11, 12], for infinite Reynolds number the boundary layer first breaks down locally at time $t = 0.75$ at an angular position 69 degrees from the rear symmetry plane.

It is seen that the computational results are in reasonable agreement with the predictions for infinite Reynolds number, despite the relatively low Reynolds number in the computation. Similarly, the predicted asymmetrical local thickening of the boundary layer that gives rise to the break-up is clearly evident.

Figure 10 shows a vortex pair bouncing off a circular cylinder. This is an illustration of the capability of our method to track separated vorticity without artificial diffusion or any need for a solution-adaptive mesh generation. Our method only locates mesh points in the regions where there is vorticity. There are no mesh points in the regions devoid of vorticity. There is no explicit mesh generation involved; our computation simply creates vorticity at the wall as required for no slip. The method then automatically extends a mesh from the cylinder out into the field, when the vorticity diffuses there. Our method uses any available computational points within the two incoming vortices when it encounters them. There is no interpolation of the solution to computational meshes or remeshing that can introduce false numerical diffusion.

We have extended the redistribution method to three-dimensional flow. The procedures are three-dimensional versions of those used in two dimensions. In particular, no problems were encountered with the larger size of the redistribution equations.

Figure 11 compares the results for diffusion of a vortex dipole with the exact solution. There is excellent agreement. Figure 12 shows the diffusion of a vortex ring. Despite the random point locations, the ring is perfectly circular.

1.3 The unsteady drag crisis.

Figure 5 compares recent values for the drag coefficient for flow about an impulsively circular cylinder at later times. It is noted that the various results disagree appreciably around time $t = 2$. Physically, at this time the Van Dommelen & Shen separation process [11, 12], which for infinite Reynolds numbers would occur at time $t = 1.5$, has caused the boundary layer to roll up into discrete vortices. As predicted by the analytical structure of the process, the evolution is quite violent.

A question of considerable interest is the initial effect of unsteady separation on the aerodynamic forces. In particular, it would be important to know whether these forces, or by implication the vehicle dynamics, can give early warning of the forming separation. Unfortunately, it has been believed since the inception of boundary layer theory that the boundary layer development cannot be directly related to the aerodynamic forces. In particular the pressure drag would require evaluation of second order effect. This seemed to make the problem of relating the Van Dommelen & Shen process to actual forces prohibitively complex.

However, in our investigation we discovered a more accurate expression for the aerodynamic forces that allows a better analysis of the theoretical properties of the drag [22]. Although the expression had been used in a more limited form in earlier work, its application to boundary layer drag had not been realized before. The new expression allowed us to evaluate the effect of the initial separation on the aerodynamic forces. In particular, we found the somewhat disappointing result that the net forces are not affected. Thus localized sensors seem required to detect separation early.

1.4 Structured Lagrangian scheme

An investigation was also conducted into advanced schemes for structured Lagrangian computations, in addition to the mesh-free scheme discussed in the previous sections. Under certain conditions, a structured scheme can have significant advantages. An example is in Lagrangian boundary layer computations of unsteady separation.

Yet iterative methods, based on the symmetric zigzag procedure of Van Dommelen & Shen [11], even enhanced with full multigrid, are very slow for the Lagrangian problem. And most conventional factorization procedures for

the 3D compressible Navier-Stokes equations are not stable for a Lagrangian computation.

An exception is a first order time-split backward-time scheme proposed by Yanenko. However, when applied to the Lagrangian boundary layer equations, this scheme proved to suffer from a considerable factorization error. Despite considerable effort, we did not succeed in obtaining sufficient accuracy at an acceptable time step using this scheme.

Hence we developed a new ADI factorization specifically for the Lagrangian problem [18]. In the scheme, the troublesome hyperbolic terms are grouped together. While this would ordinarily defeat the purpose of the ADI factorization, by selecting a bidiagonal discretization of the incremental solution, we obtained a scheme in which an iterative procedure converges almost instantaneously. In two dimensions, the scheme is significantly better than any other Lagrangian boundary layer scheme used before, by us or others, and unlike the earlier schemes it has no additional difficulties in three dimensions.

1.5 Second order boundary-layer theory

In order to understand the limitations of boundary layer theory, second order boundary layer theory is needed. It shows how relevant boundary layer theory is for a given Reynolds number and time, and how the Navier-Stokes results approach the boundary layer ones for increasing Reynolds number. These issues are essential to understand the form that the Van Dommelen & Shen process takes at finite Reynolds numbers.

For that reason, we developed a new code that computes the second order boundary layer solution. To be precise, it computes the first and second order boundary layer solutions together. In order to simplify the boundary conditions for the second order boundary layer solution above the boundary layer, a vorticity formulation was used. In order to prevent the numerical triggering of short wave length instabilities in the boundary layer, upwinding is undesirable. Instead a zigzag scheme was used with reversal of the forward direction at each time step. For stability reasons, the vertical velocity component was further staggered in the streamwise direction. The finite difference equations were time-linearized and solved using a block tridiagonal solver. [21, 23].

Figure 13 shows the shear on the rear of a circular cylinder at a time still

well before separation. It is seen that all available results, except those of Cebeci [1] agree about the correct wall shear at this time. Our new method proves to be very efficient, and gives the same results at mesh sizes 256×128, 512×256, and 768×384. Such convergence continues to times very close to separation.

Some of the other results are shown in figures 6 and 7 . It was found that the second order solution introduces short scale phenomena into the flow. This appears to agree with the analytical results of Cowley, Van Dommelen, and Lam [3] and with the numerical solution of the asymptotic interaction problem by Degani, Walker & Smith [4]. In particular, the second order effects may explain the formation of the secondary eddies near unsteady separation. There is therefor no new physics required to explain these secondary vortices beyond the Van Dommelen and Shen separation process.

References

[1] Cebeci, T. (1986) Unsteady boundary layers with an intelligent numerical scheme. *J. Fluid Mech.* **163**, 129-140.

[2] Collins, W. M. & Dennis, S. C. R. (1973) The initial flow past an impulsively started circular cylinder. *Quart. J. Mech. Appl. Math.* **26**, 53-75.

[3] S. J. Cowley, L. L. Van Dommelen, and S. T. Lam (1990) "On the use of Lagrangian variables in unsteady boundary–layer separation", *Phil. Trans. R. Soc. Lond.* A**333**, 343-378.

[4] Degani, A. T., Smith, F. T., and Walker, J. D. A. Submitted to the *J. Fluid Mech.*

[5] Koumoutsakos, P. & Leonard, A. (1995) "High-resolution simulation of the flow around an impulsively started cylinder using vortex methods", *J. Fluid Mech.* **296**, 1.

[6] Shankar, S. & Van Dommelen, L. (1994) A redistribution technique for vortex methods. Presented 47th Ann. Meet. Div. Fluid Dynamics, Am. Phys. Soc., Atlanta, GA.

[7] Shankar, S., Wang, S.-C. & Van Dommelen, L. L. (1995) Simulating diffusion in vortex methods using a vorticity redistribution technique. Forum on Vortex Methods for Engineering Applications, Feb. 22-24 1995, Albuquerque, NM. 107-124.

[8] Shankar, S. & Van Dommelen, L. (1995) A new diffusion scheme for vortex methods for three-dimensional incompressible flows. 2nd International Workshop on Vortex Flows and Related Numerical Methods, Montreal, Canada, August 20-24, (1995).

[9] Shankar, S. & Van Dommelen, L. L., (1995) A new diffusion procedure for vortex methods. Submitted to the *Journal of Computational Physics.*

[10] Shih, C., Lourenco, L., Van Dommelen, L. & Krothapalli, A. (1992) Unsteady flow past an airfoil pitching at a constant rate. *AIAA Journal* **30** 1153-1161. (A combined experimental, numerical, and theoretical study of unsteady stall of wings).

[11] Van Dommelen, L. L. & Shen, S. F. (1980) The spontaneous generation of the singularity in a separating laminar boundary layer. *Journal of Computational Physics* **38** 125-140.

[12] Van Dommelen, L. L. & Shen, S. F. (1982) The genesis of separation. In *Symposium on Numerical and Physical Aspects of Aerodynamic Flows,* (T. Cebeci, Ed.) 293-311. Springer-Verlag.

[13] Van Dommelen, L. L. & Shen, S. F. (1985) The flow at a rear stagnation point is eventually determined by exponentially small values of the velocity. *Journal of Fluid Mechanics* **157** 1-16.

[14] Van Dommelen, L. L. and Rundensteiner, E. A. (1989) Fast, adaptive summation of point forces in the two-dimensional Poisson equation, *J. Comput. Phys.* **83**, 126.

[15] Van Dommelen, L. L. (1989) A Vortex Redistribution Technique, Florida State University, Department of Mechanical Engineering, Report FMRL TR-3, (unpublished).

[16] Van Dommelen, L. L. (1989) Some experiments on a vortex redistribution method, American Mathematical Society regional meeting, Hoboken, NJ, Oct 21-22.

[17] Van Dommelen, L. L. & Cowley, S. J. (1990) On the Lagrangian description of unsteady boundary layer separation. Part 1. General theory. *Journal of Fluid Mechanics* **210** 593-626.

[18] Van Dommelen, L. L. (1993) Lagrangian computation of 3D unsteady separation. International Workshop on Advances in Analytical Methods in Aerodynamics, Miedzyzdroje, Poland, July 12-14, 1993.

[19] Van Dommelen, L. L. & Wang, S.-C. (1994) Determining unsteady 2D and 3D boundary layer separation. Symposium on Aerodynamics and Aeroacoustics (ed. K. Y. Fung), 187-206. World Scientific Publishing.

[20] Van Dommelen, L. L. & Shankar, S. (1995) Two counter-rotating diffusing vortices. *Physics of Fluids* **7** 808-819.

[21] Van Dommelen, L. L. (1995) Second order effects on unsteady separation. Presented 48th Ann. Meet. Div. Fluid Dynamics, Am. Phys. Soc., Davis, CA.

[22] Van Dommelen, L. L. & Shankar S. (1996) Aerodynamic forces are not affected by initial separation. Submitted to the *Physics of Fluids*.

[23] Van Dommelen, L. L. & Shankar, S. (1995) The separation singularity at infinite and finite Reynolds numbers, In preparation.

[24] Van Dommelen, L. (1995) Note on inviscid singularities and turbulence. Submitted to the Journal of Fluid Mechanics.

[25] Wang, S.-C. (1995) Control of dynamic stall. Ph.D. thesis, FAMU-FSU College of Engineering, Tallahassee, FL.

Impulsively started flow past a NACA0012 airfoil : Re = 5000

a.

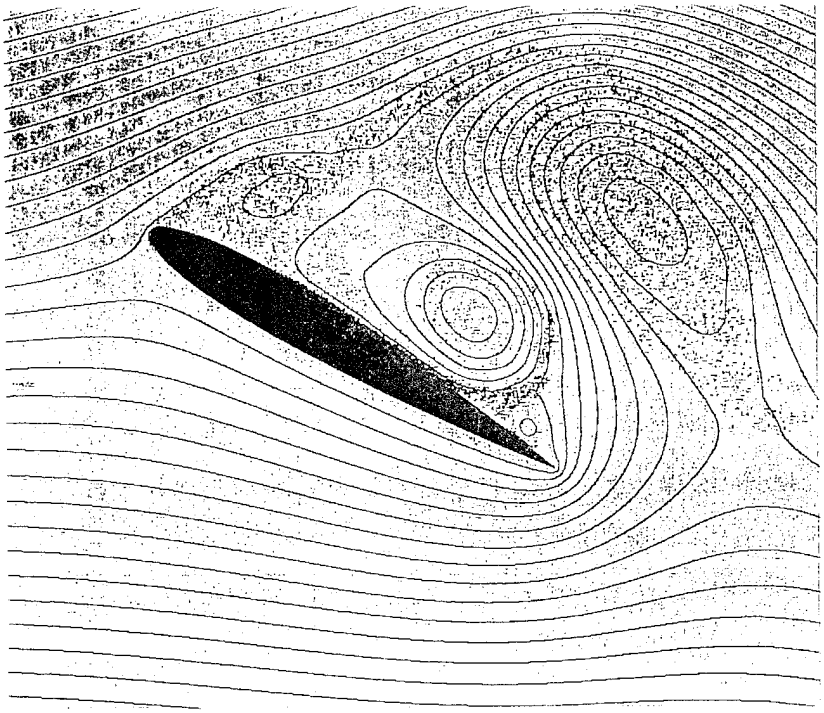

b.

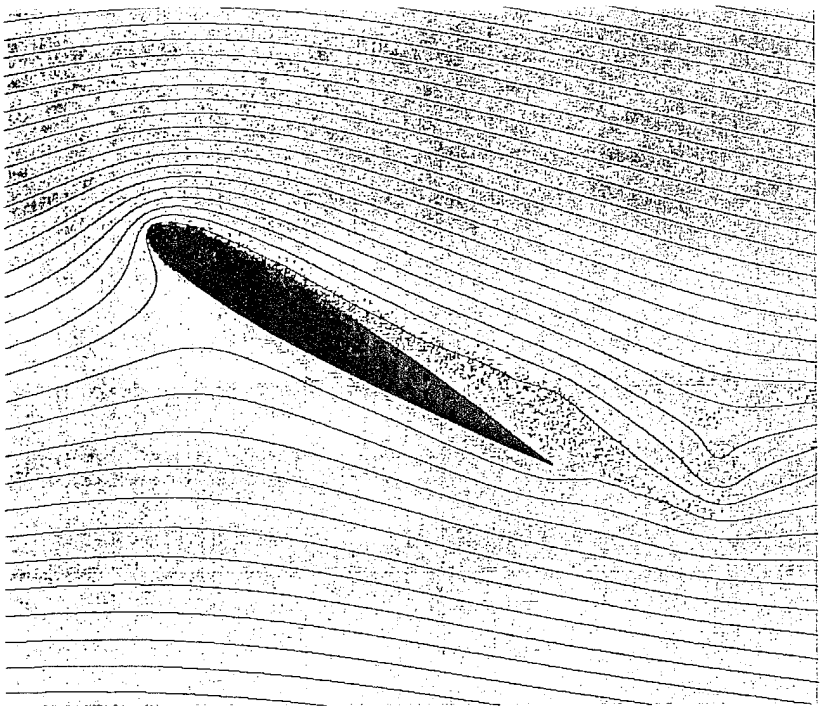

Figure 1. (a) Flow without suction ; (b) Flow with suction.

Vortex density for Re = 50

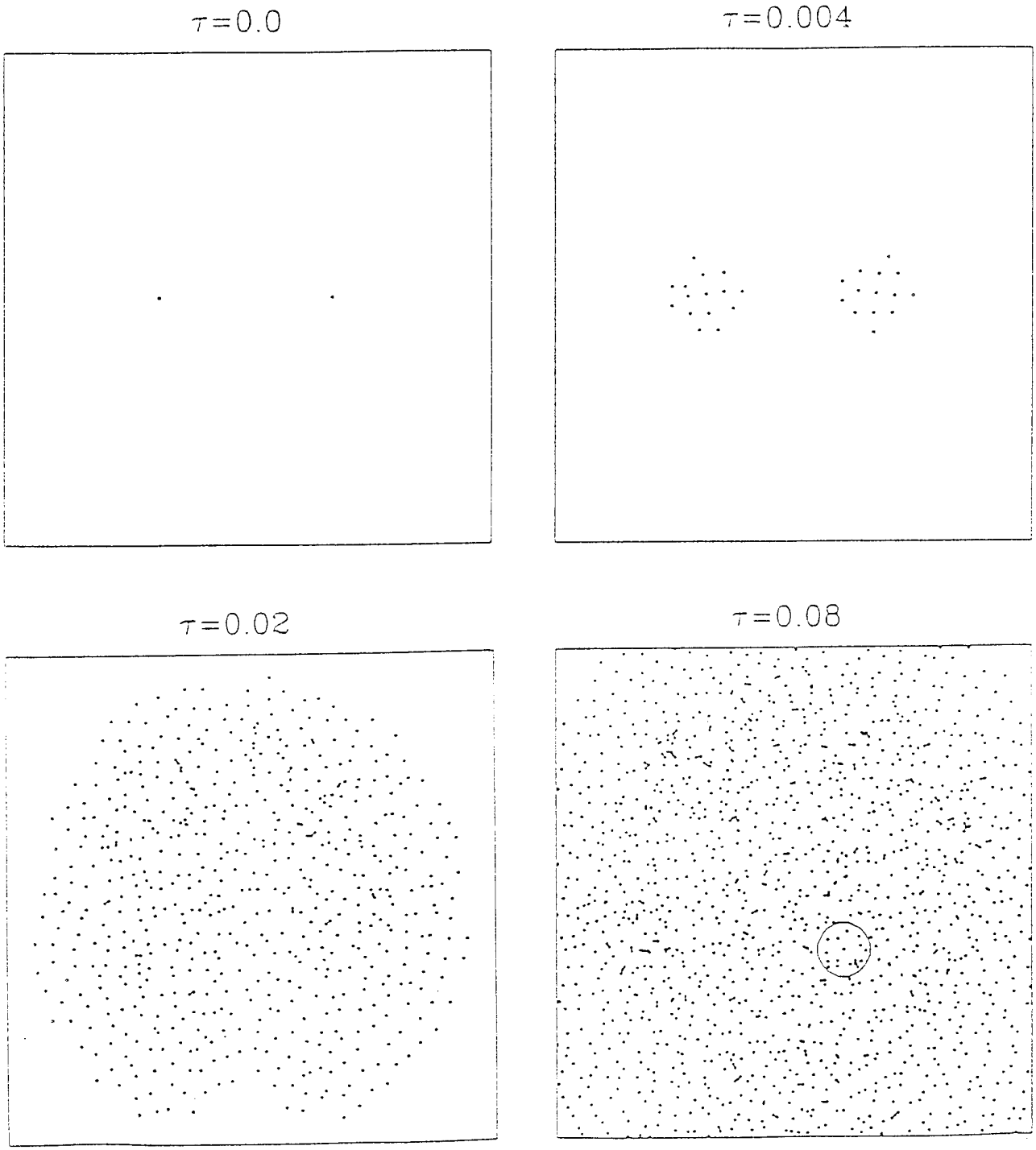

Figure 2

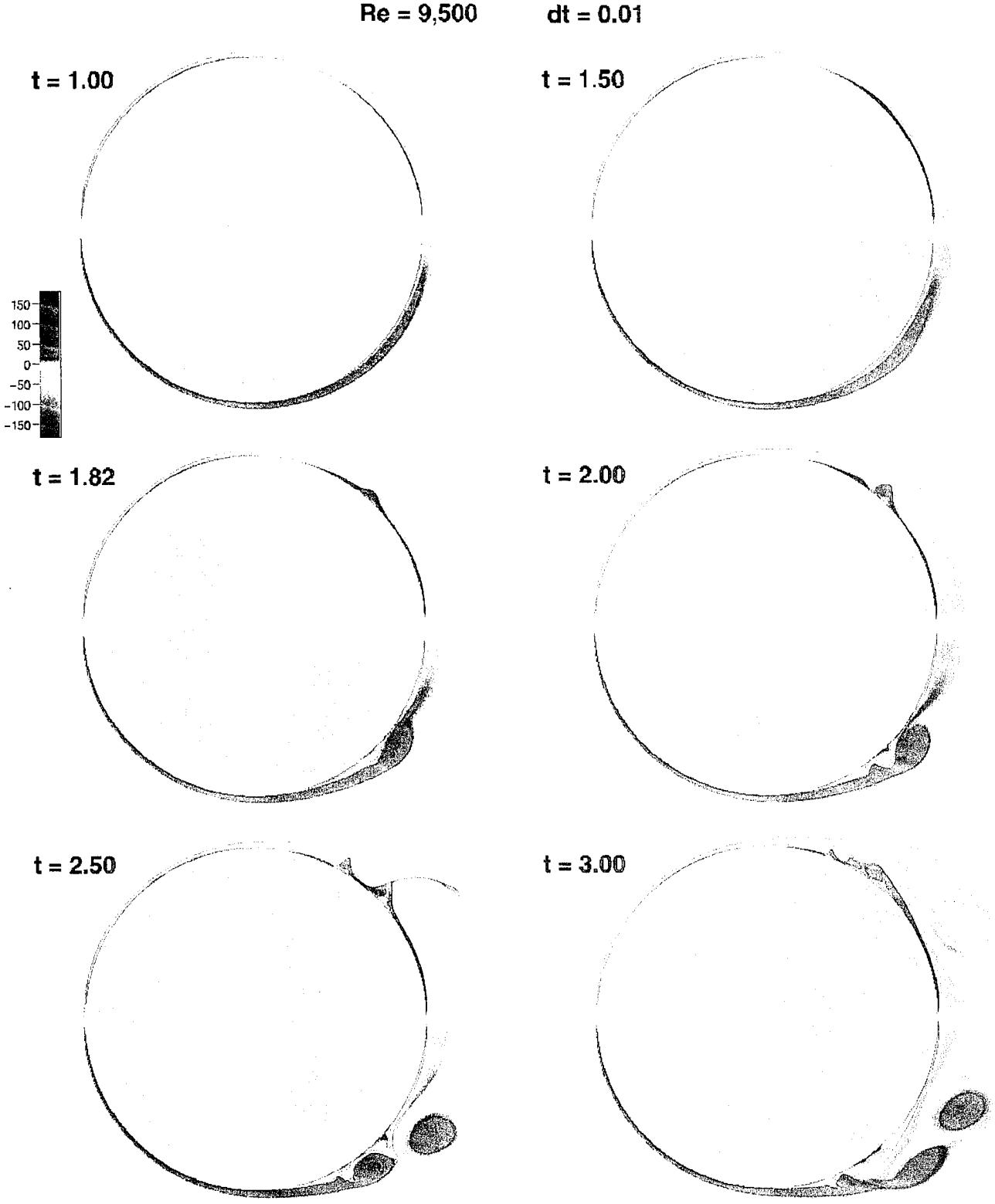
Re = 9,500
dt = 0.01
t = 1.00
t = 1.50
150
100
50
0
-50
-100
-150
t = 1.82
t = 2.00
t = 2.50
t = 3.00

Figure 3

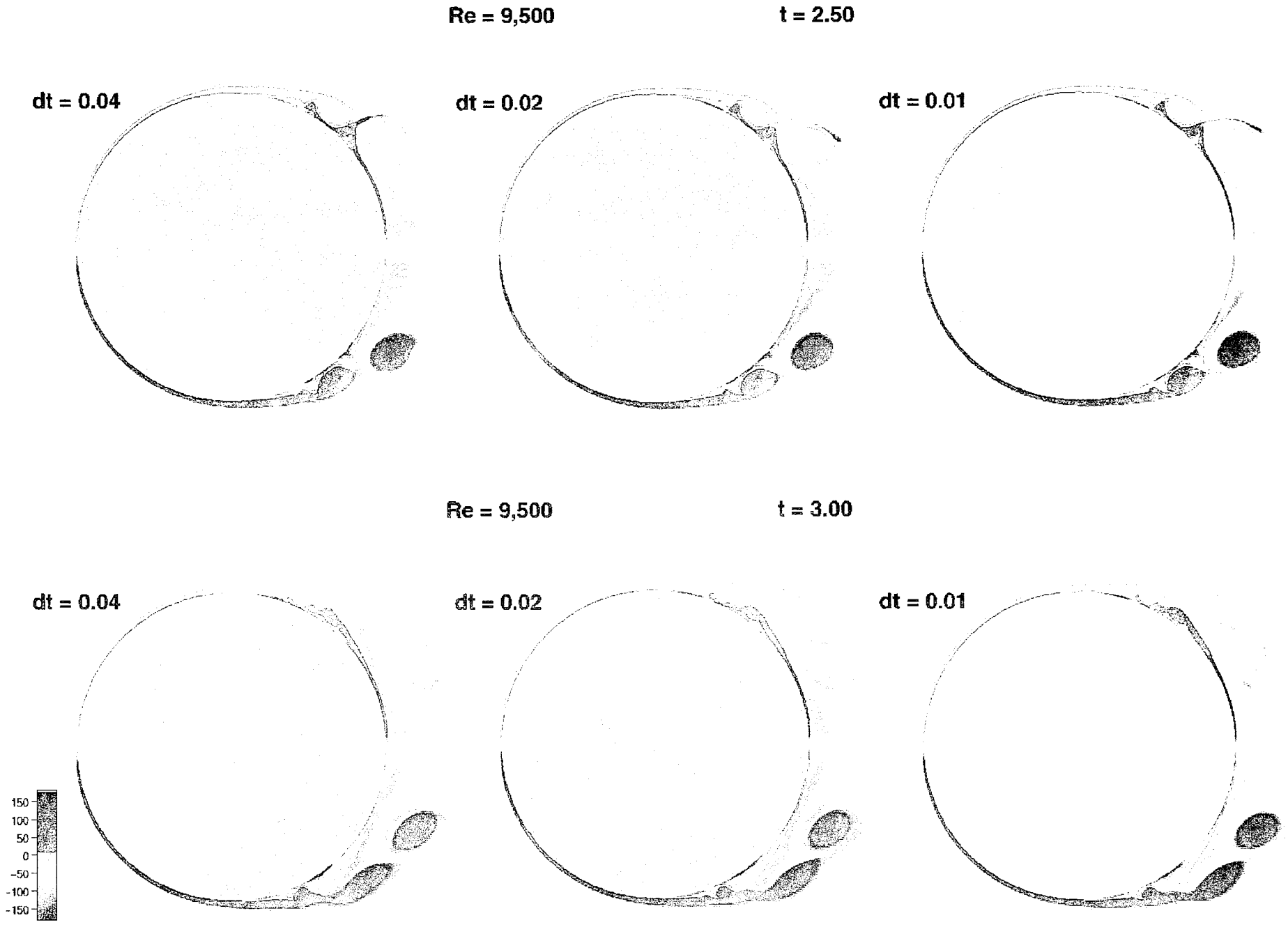
Re = 9,500
t = 2.50
dt = 0.04
dt = 0.02
dt = 0.01
Re = 9,500
t = 3.00
dt = 0.04
dt = 0.02
dt = 0.01
150
100
50
0
-50
-100
-150

Figure 4

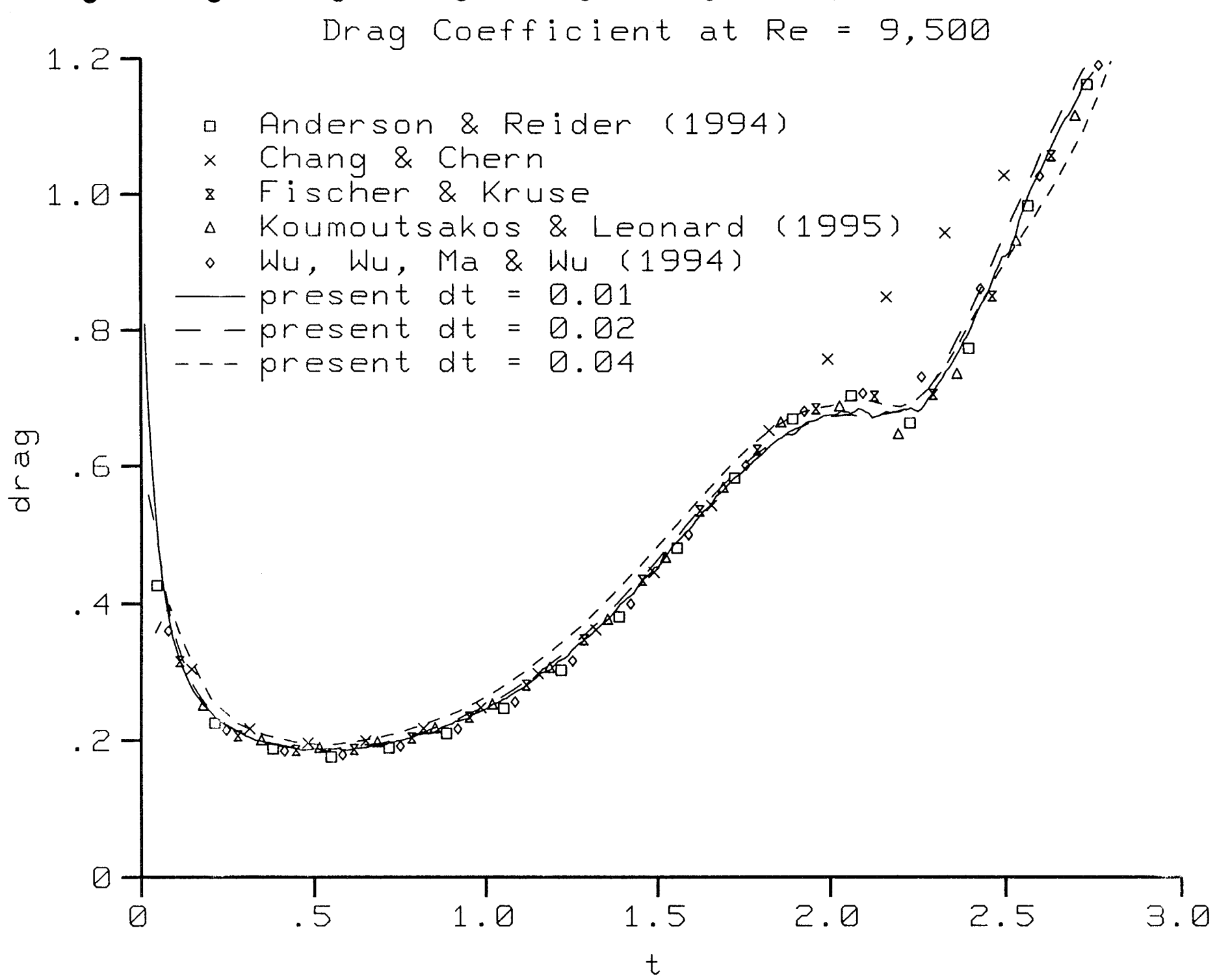
Drag Coefficient at Re = 9,500
Anderson & Reider (1994)
Chang & Chern
Fischer & Kruse
Koumoutsakos & Leonard (1995)
Wu, Wu, Ma & Wu (1994)
present dt = 0.01
present dt = 0.02
present dt = 0.04
drag
t
1.2
1.0
.8
.6
.4
.2
0
0
.5
1.0
1.5
2.0
2.5
3.0

Figure 5

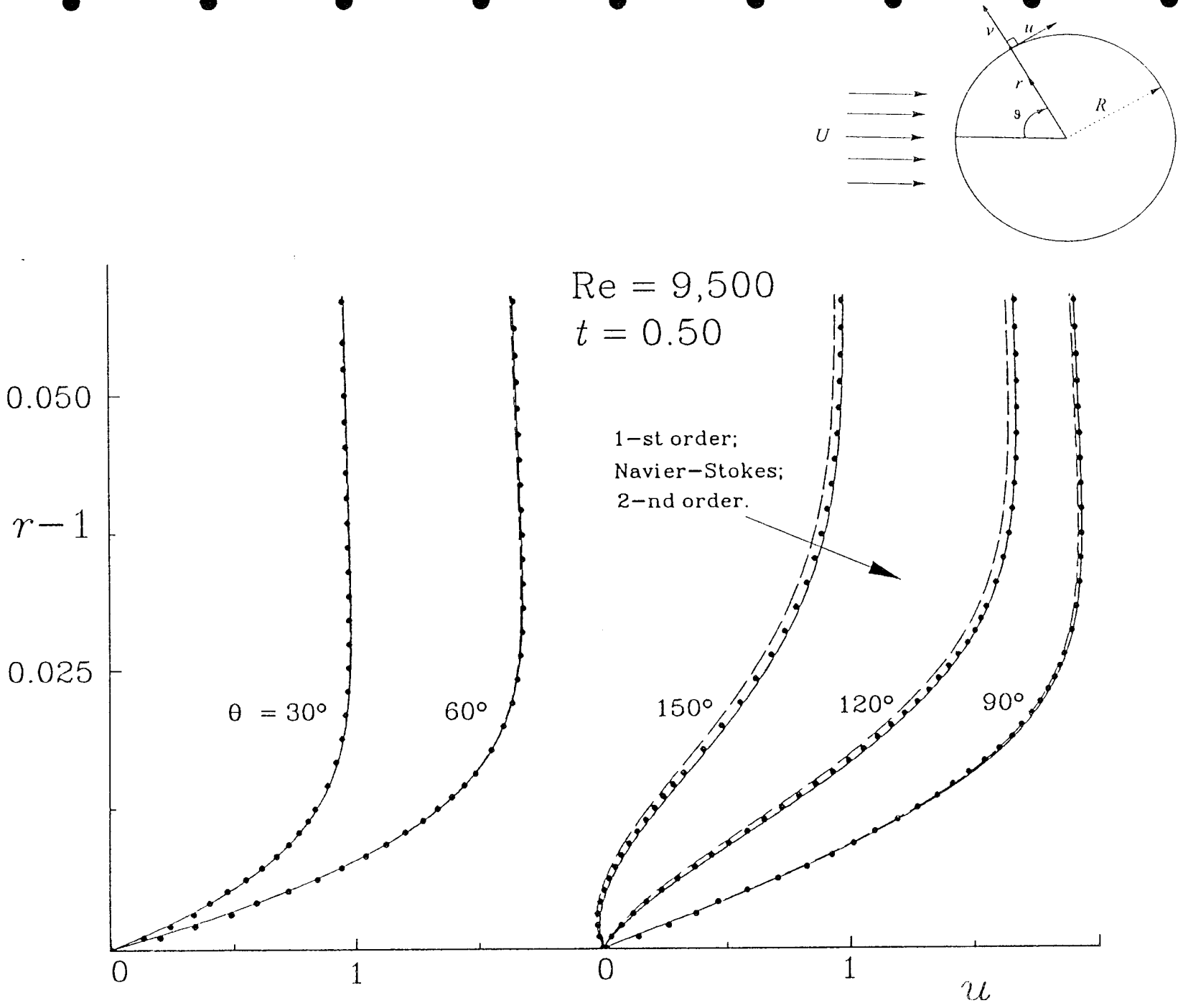
v
u
r
9
R
U
Re = 9,500
t = 0.50
0.050
r − 1
0.025
1−st order;
Navier−Stokes;
2−nd order.
θ = 30°
60°
150°
120°
90°
0
1
0
1
u

Figure 6

Drag coefficient

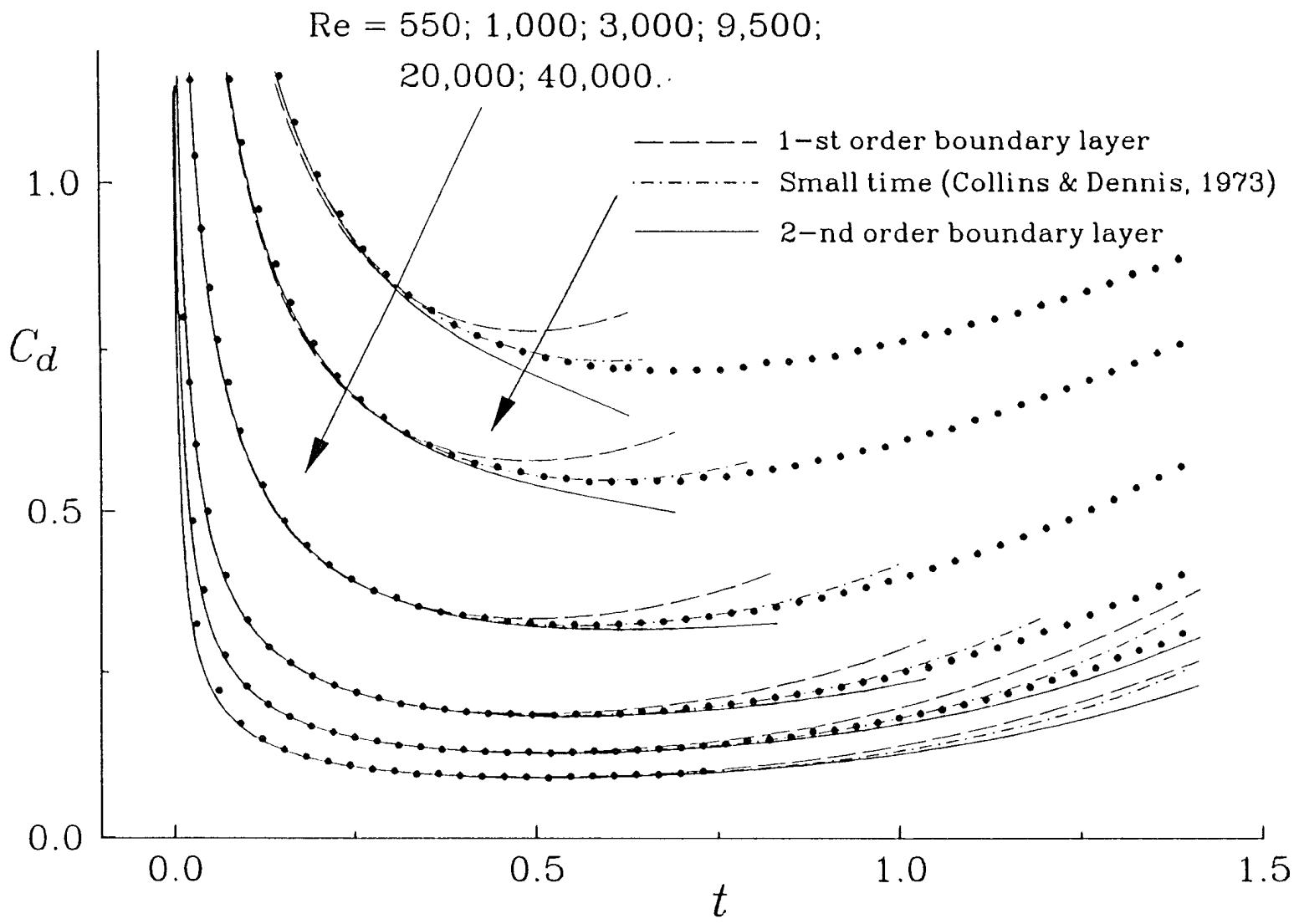

Figure 7

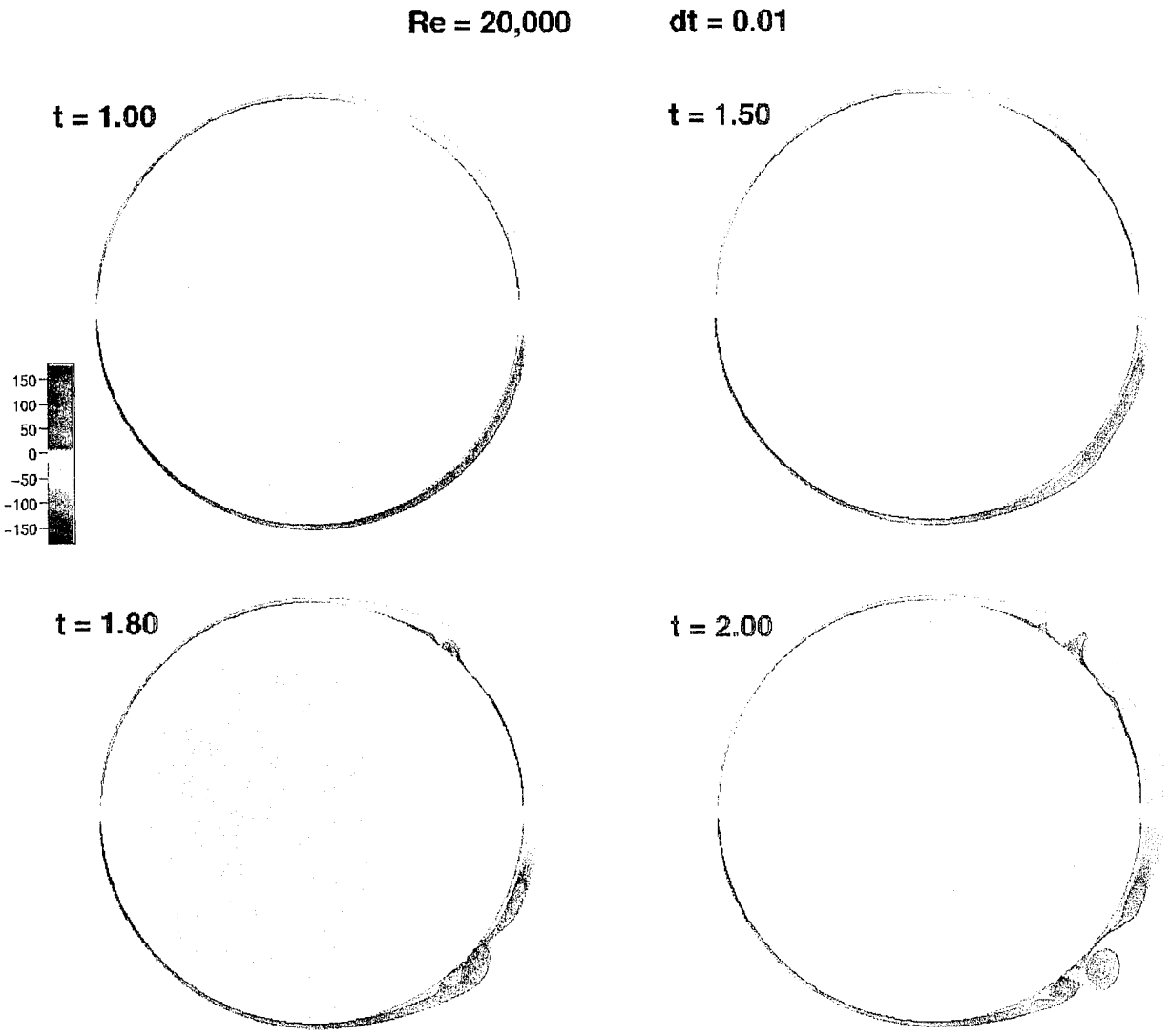

Figure 8

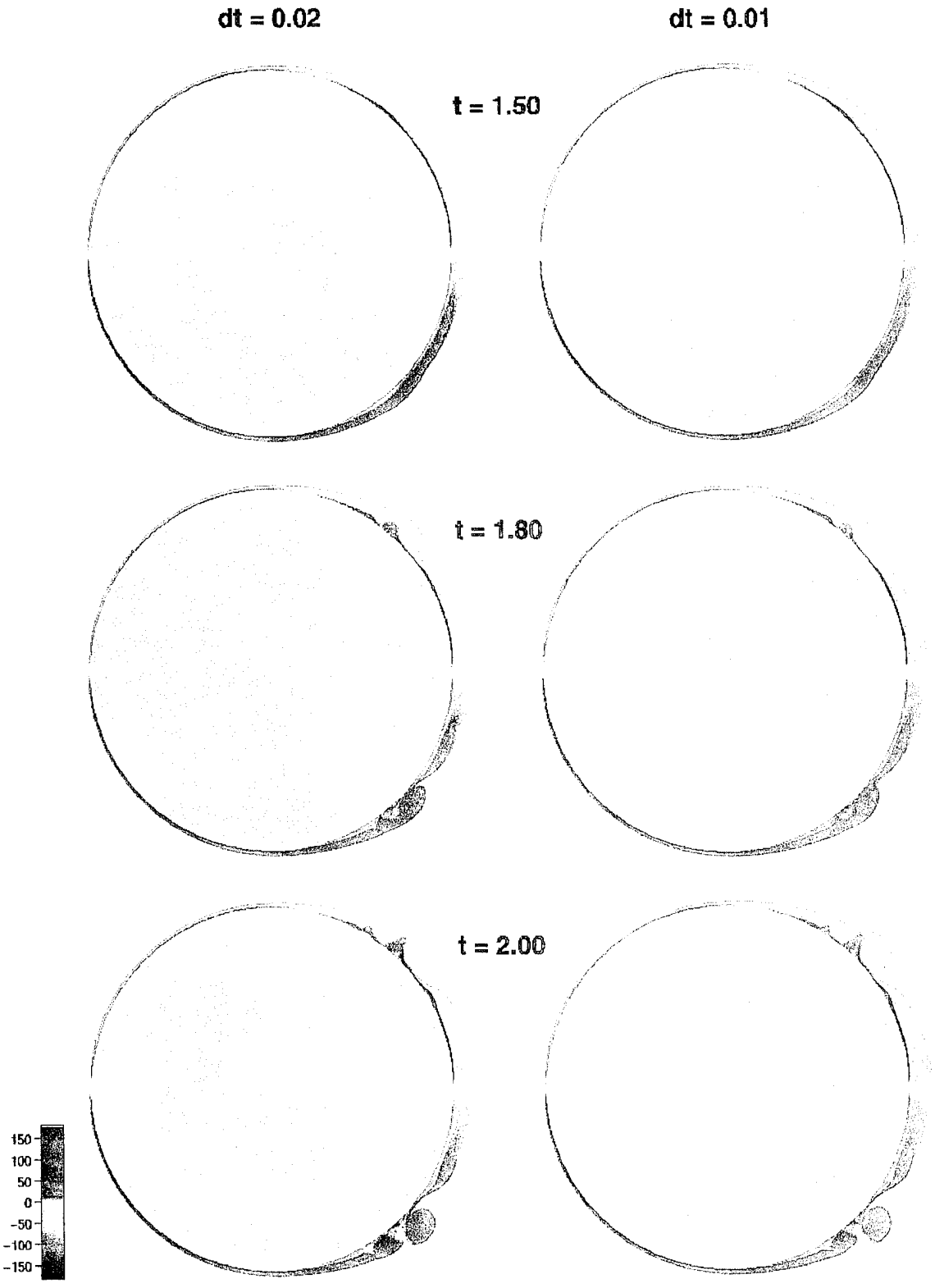

Figure 9

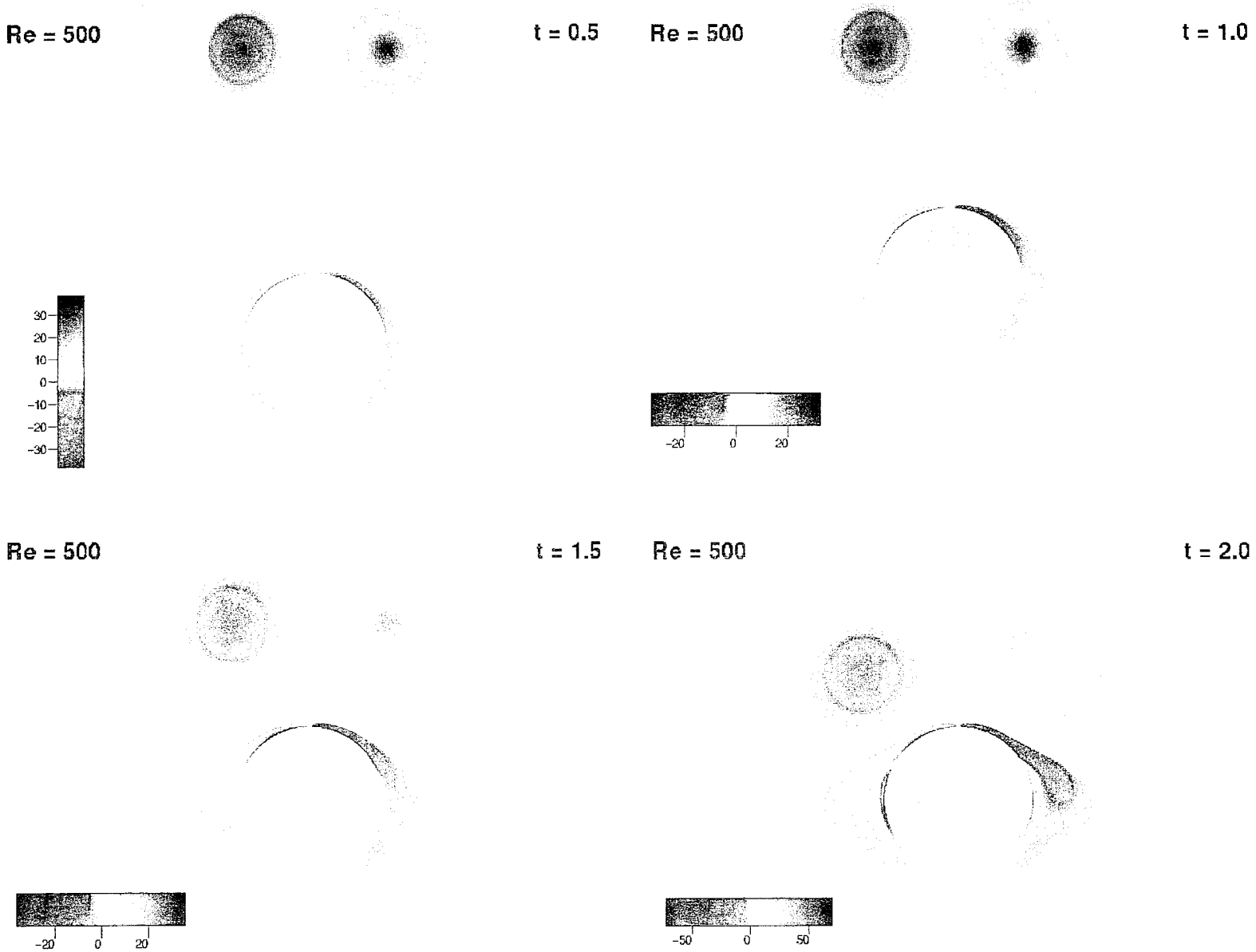
Re = 500
t = 0.5
Re = 500
t = 1.0
30
20
10
0
-10
-20
-30
-20
0
20
Re = 500
t = 1.5
Re = 500
t = 2.0
-20
0
20
-50
0
50

Figure 10

Re = 500 t = 2.5

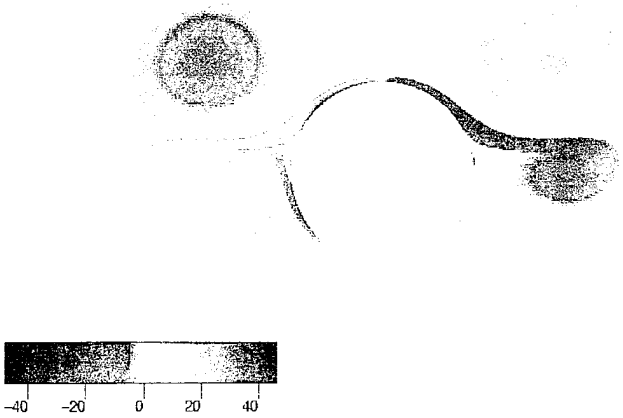

Re = 500 t = 3.0

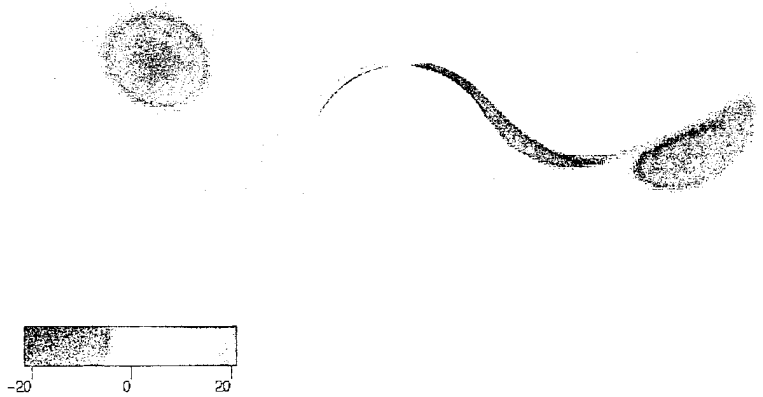

Re = 500 t = 3.5

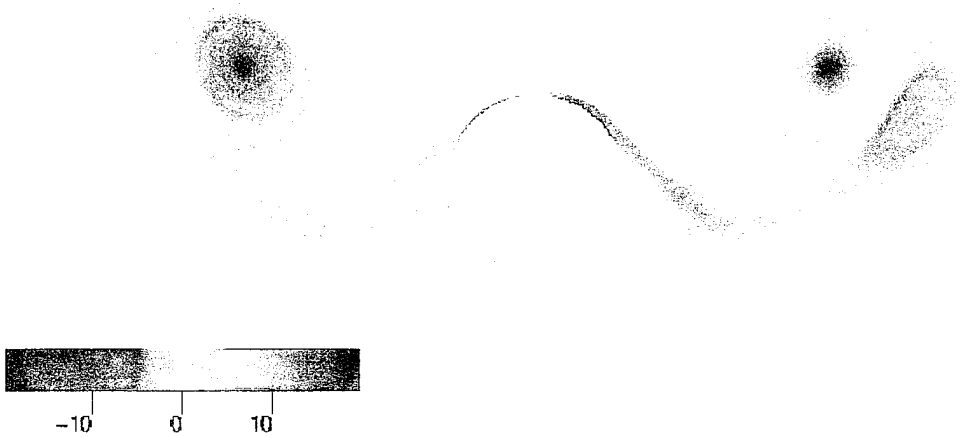

Diffusing dipole in 3-D

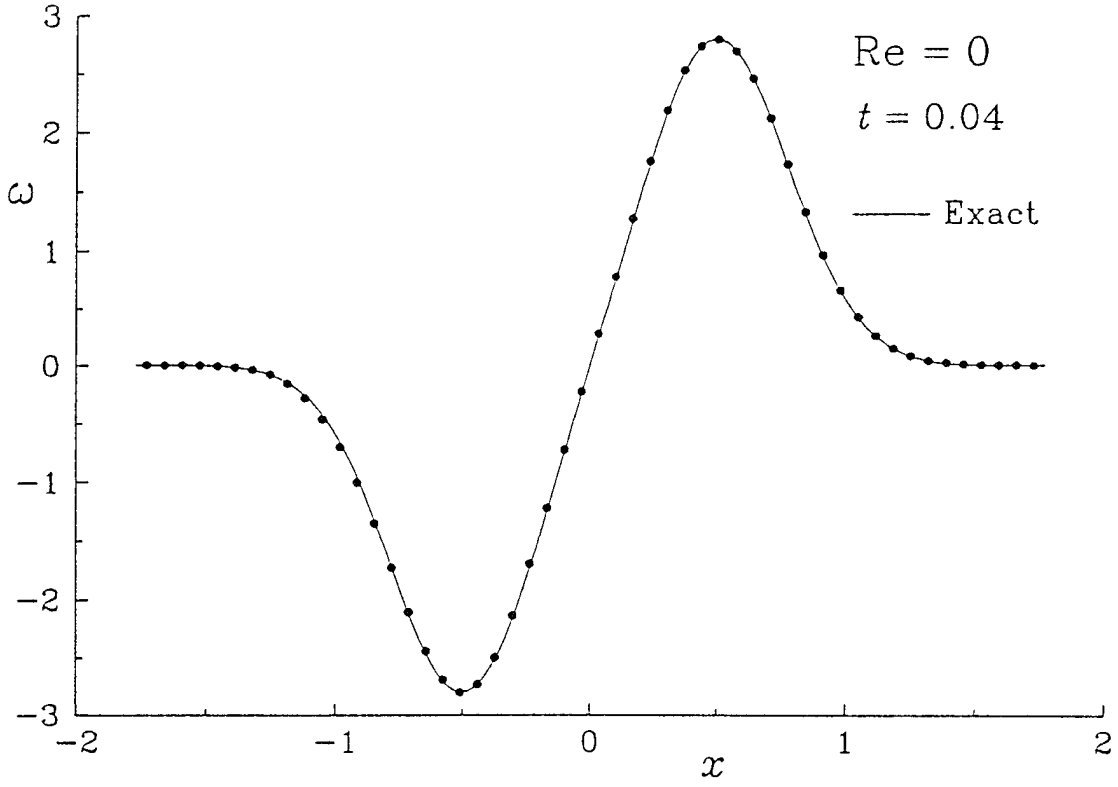

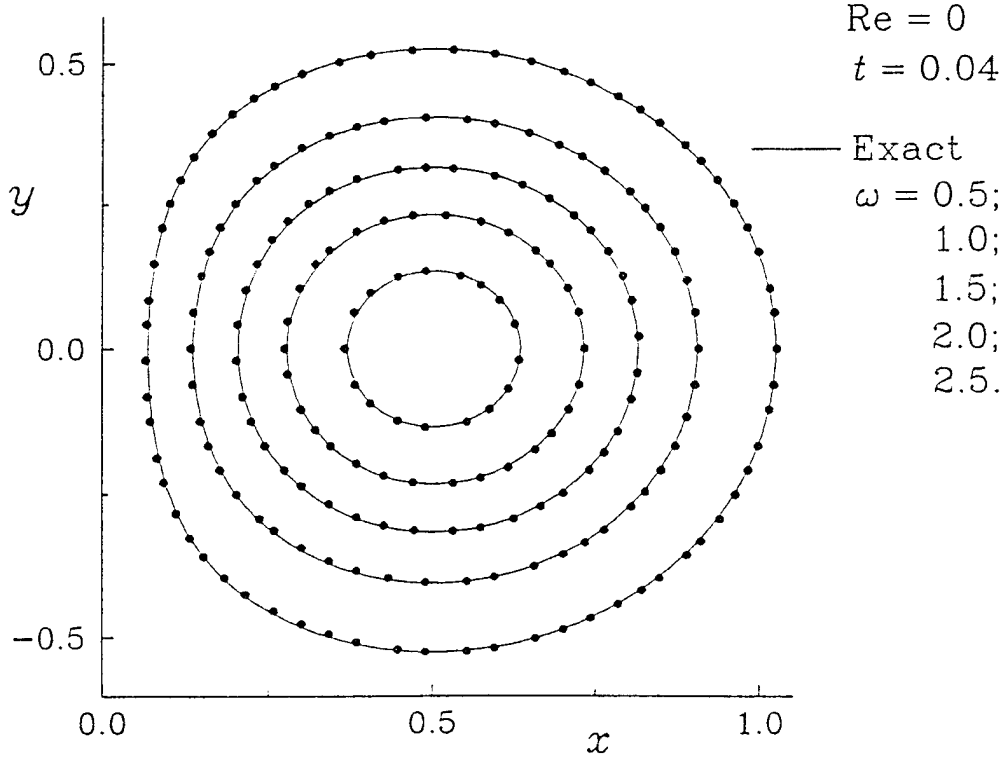

Figure 11

Diffusing vortex ring: Re = 0

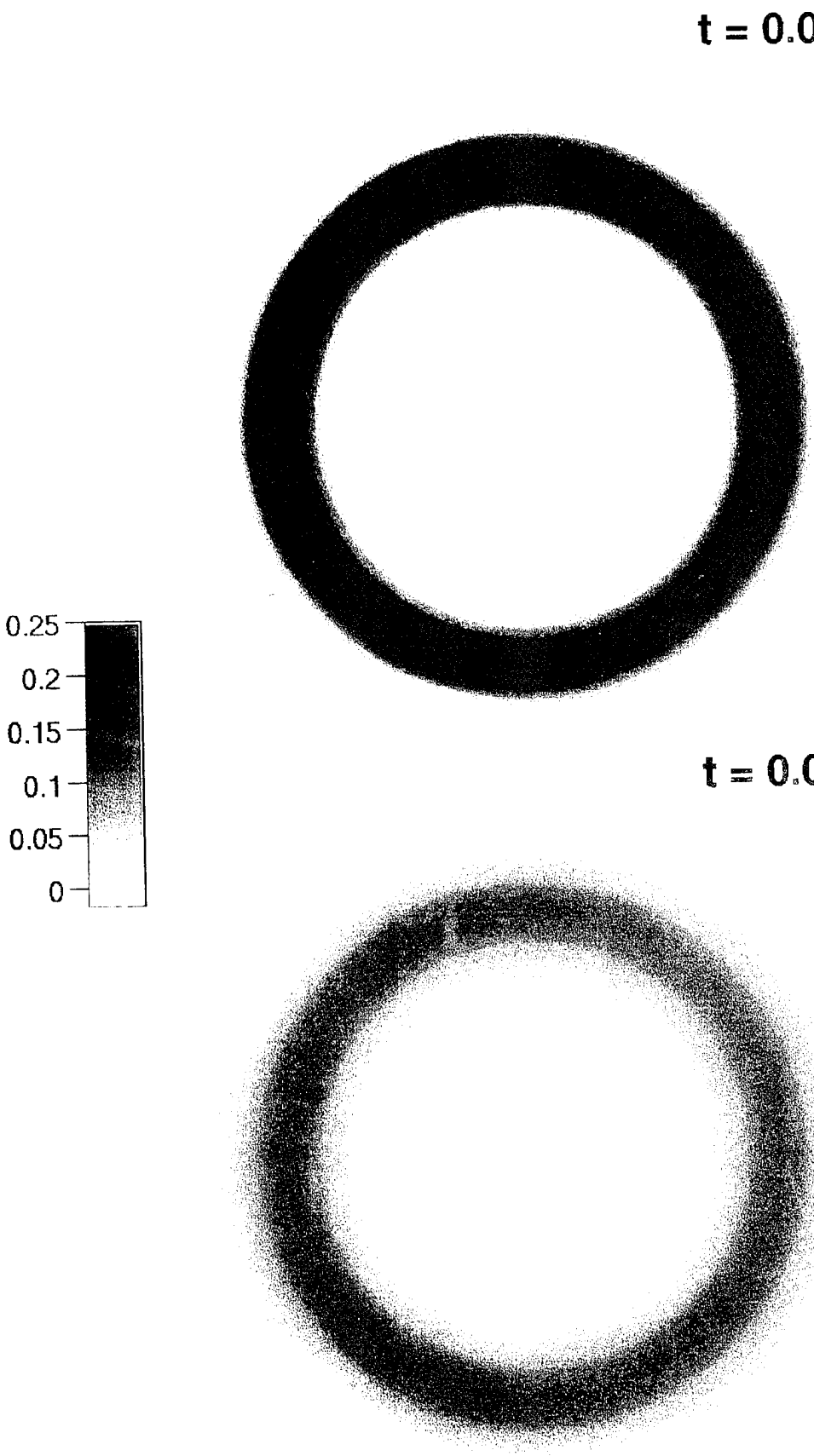

Figure 12

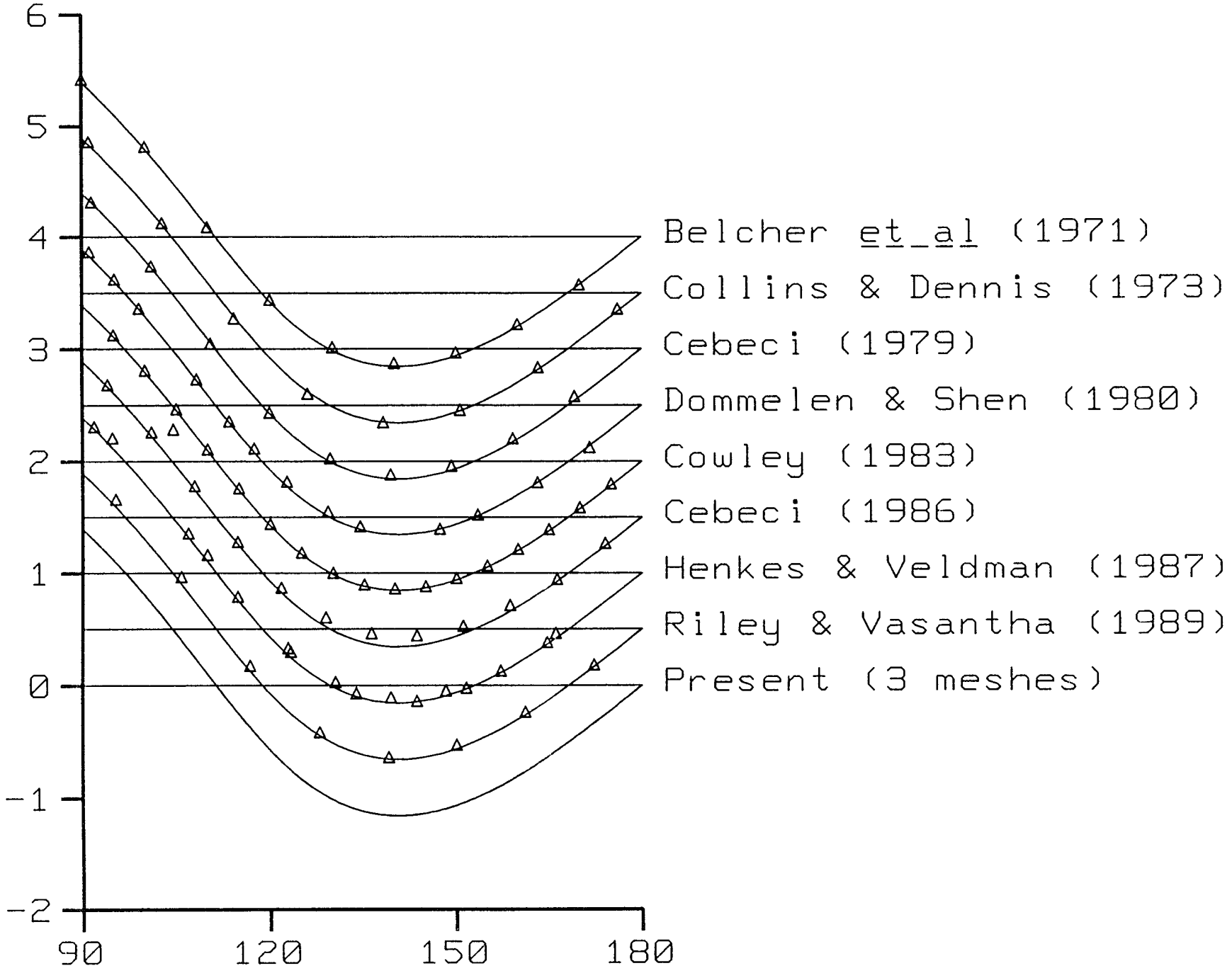
6
5
4
3
2
1
0
-1
-2
90
120
150
180
Belcher et al (1971)
Collins & Dennis (1973)
Cebeci (1979)
Dommelen & Shen (1980)
Cowley (1983)
Cebeci (1986)
Henkes & Veldman (1987)
Riley & Vasantha (1989)
Present (3 meshes)

Figure 13

2. Experimental Research

The experiments are performed in a water towing tank facility with dimensions of 3.6 m in length and 0.55 x 0.42 m^2 in cross section. A computer-interfaced Anorail linear motor system is used to drive the towing carriage. This system allows for fine control of the towing velocity. The Reynolds number, based upon the wing's root chord (C) and the free stream velocity (U_∞), can be varied from 5,000 to 25,000. The wing's pitching motion is controlled by a programmable "Klinger" stepping motor control unit. All motions are coordinated using a desktop IBM PS/2 model 70 computer. Three moving platforms, one for model-mounting, one for the rotating mirror system used to create the pulsed laser illumination, and the other for image recording, are synchronized using a gear/belt system (figure 1). A 1/4-hp aquarium pump that is connected to a 30 gallon reservoir tank is used for the trailing edge jet flow control. Two rectangular jet nozzles, each of which with its own supply line, are located at the trailing edge of the wing for control purpose.

The delta wing model has a leading edge sweep angle of 60^o and a root chord of 13.0 cm. The Reynolds number is 9,800 for all cases tested. The leading edges are beveled 45^o leeward from the top surface. The model has a relatively large thickness of 2.54 cm in order to accommodate the reservoir chambers for the trailing edge jet. The model is mounted from its bottom surface using two stings. The Plexiglas stings have an exterior shape of a NACA 0015 airfoil contour to minimize the interference generated by the sting supports. Inside each of the supports, a brass tube is used to direct the flow from the pump into the settling chamber for the purpose of the jet control. Two flow control systems are located symmetric about the wing's centerline. The two control jets can be operated independently through separate system of valves and passage conduits. To ensure a uniform jet output, the flow is expanded into the settling chamber filled with foams. No noticeable non-uniformity is observed based on visual inspection of the jet flow.

The direction of the jet flow is controlled by using vectored nozzle mounted on the exit of the settling chamber (figure 2). The nozzle has a height (h) of 0.51 cm and a span (S) of 4.89 cm, which gives a 9.6 to 1 aspect ratio. Although the axis switching of the jet and the emergence of three-dimensionality is expected downstream, the near jet flow field is expected to be fairly two-dimensional. By using different nozzle configuration, the

deflection angle of the vectored jet system can be varied from upward 30^{o} to downward downward 45^{o} with respect to the surface of the wing. As shown in figure 2, the left-sided jet is directed downward at 30^{o} while the right-sided jet is point 30^{o} upward. This is the asymmetric flow control configuration used in the present investigation. Currently, the jet velocity (U_J) can be varied from 0 to 7.3 times of the free stream velocity. The strength of the jet is measured by the jet momentum coefficient, C_J:

$$C_J = J/qC, \text{ where } J=\rho U_J^2 h, \text{ and } q=1/2\rho U_\infty^2 \qquad (1)$$

The C_J is set at 4.15 for both jets in the present study. The flow rate is determined by measuring the variation of the water level inside the reservoir tank over a period of time. No appreciable variation of the supply flow rate is detected during the test.

PIV and Dye Flow Visualization Setup

For a qualitative understanding of the flow behavior, a dye flow visualization experiment is used. The development of the leading edge vortex core is tagged by dye injected via small tubes near the apex of the delta wing. Initially, the dye is trapped inside the core when the leading edge vortex is stable. The emergence of instabilities and the eventual breakdown of the vortex can be identified by the quick dispersion of the dye. A 35 mm Nikon camera, which is mounted on a platform moving with the wing, is used to record the flow visualization results for static case. For the dynamic pitching cases, a video camera is used to obtain finer temporal resolution. For the PIV measurements, the pulsed laser sheet is created by means of a 24-faceted rotating mirror system. This mirror sweeps an 18 Watt Argon laser beam into pulsed laser sheets which are projected along a selected plane on the wing, providing multiple particle image illumination required for the PIV image recording.

The Particle Image Velocimetry (PIV) technique is capable of providing two-dimensional, instantaneous velocity and vorticity fields with accuracy. Digital image processing technique is used to convert the acquired PIV photographic records into local velocity data. An optical Scanner (Nikon Coolscan) is used to scan and digitize the PIV photographic film with a very high resolution up to a maximum of 2702 pixels per inch. The electronically digitized image can then be processed using the standard Fast Fourier Transform algorithm. In the present study, the PIV velocity field is computed locally using

a small interrogation window which has an equivalent physical dimension of 1.7 by 0.85 mm, or 1.3% by 0.7% root chord length, respectively. The shorter side of the window is aligned in the direction that is normal to the freestream where the flow field has a larger gradient.

Silver coated hollow glass beads (Potter Industry), with an average diameter of 10 μm and a specific gravity of 1.3, are used as the flow tracers. A phase-triggered 35 mm SLR camera (Nikon F-3) is used to record the image at a controllable rate, ranging from 1 frame/sec to a maximum rate of 6 frames/sec. Synchronization between components is accomplished using a Counter/Timer processor interfaced to a Macintosh II computer. This system also provides the phase-reference between the motion of the wing and the PIV photographic timing sequence.

Results and Discussion

From the qualitative dye flow visualization, it has been shown that a vectored, trailing edge jet has a significant effect in delaying the vortex breakdown on a high angle of attack delta wing (figure 3). Strong asymmetric bursting of the leading edge vortices can be induced by arranging the vectored jet in an asymmetric configuration (figure 4). The effectiveness of the trailing edge jet control strongly depends on the jet velocity and the control nozzle angle. Higher jet velocity and larger downward nozzle angle with respect to the free-stream provide more effective stabilizing effect on the leading edge vortex system. Transient pitching motion can also significantly delay the onset of the vortex breakdown. The higher the pitch rate, the higher angle of attack the leading edge vortex will experience a local breakdown. Compared to the pitching motion, the favorable effect produced by the jet has relatively less influence on the propagation of the vortex breakdown. Efforts had also been made at the implementation of the PIV technique to characterize the cross stream flow field of the leading edge vortex system with and without the presence of the vectored jet. Instantaneous velocity and associated vorticity fields had been obtained using PIV with a special emphasis on the understanding of the flow instabilities along the vortex core at the onset of the vortex breakdown. The instantaneous leading edge vortices show a quasi-periodic oscillation before they undergo breakdown (figure 5). Strong interaction between the primary vortex and the secondary vortex plays an important role on the onset of breakdown. With jet control, an accelerated flow along the vortex axis increases the transportation of vorticity along the vortex core. Consequently, the vortex structure can be stabilized to higher angle of attack compared to its uncontrolled counterpart (figure 6).

Most of the results had been presented in 1994 APS Fluid Dynamics Meeting[1], 1995 AIAA Meeting[2], and 1995 APS Fluid Dynamics Meeting[3]. A more detailed documentation of the aforementioned studies is included in a paper[4] which is scheduled to be published in AIAA Journal.

The investigation of the vortex breakdown phenomenon of the flow over a 75° sweep delta wing had been presented in 1996 AIAA Reno Meeting[5]. This study emphasizes on the detailed measurement of the cross stream flow field of the leading edge vortices at both static and dynamic conditions. Vortex breakdown characteristics measured using PIV are then compared to that of a 60° sweep wing. Significant differences had been found between these two flow fields. A quasi-periodic shedding of Kelvin-Helmholtz type eddies from the separated shear layer is measured using whole-field PIV technique (figure 7). This shedding appears to be related to the primary vortex/boundary layer interaction and the eruption process of the secondary structure under the induction of the primary vortex. Similar interaction and the associated strong vortex instability has also been observed in a 60° sweep angle delta wing flow field (figure 5). Along the vortex axis, the velocity distribution changes from a jet type profile to a wake type profile (figure 8), signifying the onset of the vortex breakdown. PIV data shows that a spiral type vortex breakdown dominates and the spiral of the vortex line is oriented spatially in a sense that is opposite to the base flow, however, it rotates in the same direction as the base flow (figure 9).

Dynamic stall phenomenon due to the leading edge boundary layer separation is also studied. Most of the results can be found in two AIAA journal papers[6,7]. These studies focus on the detailed measurement of the unsteady separated flow in the vicinity of the leading and trailing edges of a two-dimensional NACA 0012 airfoil. Near the leading edge, large scale vortical structures emerge as a consequence of van Dommelen and Shen (VDS) type separation and a local vorticity accumulation. The interaction of these vortices with the reversing boundary-layer vorticity initiates a secondary flow separation and the formation of a secondary vortex. The mutual induction of this counter-rotating vortex pair eventually leads to the ejection process of the dynamic stall vortex from the leading-edge of the airfoil. This interaction bears qualitative similarity to the interaction between delta wing vortices and their secondary vortices discussed previously.

Another interesting observation is presented in a ASME Fluids Engineering Meeting in 1994[8]. The role of absolute instability on the formation of dynamic stall vortex of a pitching-up airfoil is examined. Due to the emergence of VDS type interaction near the leading edge, a counter-flowing free shear layer is formed as a result of the local boundary layer separation. The dynamics of the emergence of large scale vortices are found to be

related to the absolute instability of the separating shear layer. As a result of the emergence of this temporal instability, the shear layer can grow locally at a fast rate, resulting in the formation of a large vortex and the subsequent initiation of the dynamic stall process. Similar observation[9] has been made at a higher Speed case with free-stream Mach numbers of 0.23 and 0.45. The initiation of the dynamic stall process appears to be connected to the emergence of the absolute instability of the separating leading edge boundary layer.

References

[1] Z. Ding, C. Shih and L. Lourenco, "Effect of Trailing Edge Jet Control on Delta Wing Leading Edge Vortex Flow," presented at 1994 47th Annual Meeting of Division of Fluid Dynamics, American Physical Society, Atlanta, GA, Nov. 1994.

[2] Z. Ding, C. Shih & L. Lourenco, "Leading Edge Vortices of a Delta Wing Flow Field - A PIV Study," AIAA Paper 95-0652, presented at 1995 33rd Aerospace Sciences Meeting, Jan. 1995, Reno, NV.

[3] Z. Ding & C. Shih, "Dynamic Pitching-Up of a Delta Wing," will be presented at 1995 48th Annual Meeting of Division of Fluid Dynamics, American Physical Society, Irvine, CA, Nov. 1995.

[4] C. Shih & Z. Ding, "Trailing Edge Jet Control of the Leading-Edge Vortices of a Delta Wing," to appear in AIAA Journal, 1996.

[5] C. Shih & Z. Ding, "Unsteady Structure of Leading-Edge Vortices on a Delta Wing," AIAA Paper 96-0664, presented at 1996 34rd Aerospace Sciences Meeting, Jan. 1996, Reno, NV.

[6] C. Shih, L.M. Lourenco, L. van Dommelen, and A. Krothapalli, "Unsteady Flow Past an Airfoil Pitching at a Constant Rate," AIAA Journal, Vol. 20, No. 5, 1992, pp 1153-1161.

[7] C. Shih, L.M. Lourenco and A. Krothapalli, "Investigation of Flow at Leading and Trailing Edges of Pitching-Up Airfoil," AIAA Journal, Vol. 33, No. 8, 1995, pp 1369-1376.

[8] C. Shih, A. Krothapalli and L. Lourenco, "The Role of Absolute Instability on the Formation of Dynamic Stall Vortex," Proceeding ASME Fluids Engineering Summer Meeting, June 19-23, 1994, Lake Tahoe, Nevada.

[9] W. Crisler, A. Krothapalii and L. Lourenco, "PIV INvestigation of High Speed Flow Over a Pitching Airfoil," AIAA Paper 94-0533, presented in 3nnd Aerospace Seiences Meeting, Jan. 1994, Reno, NV

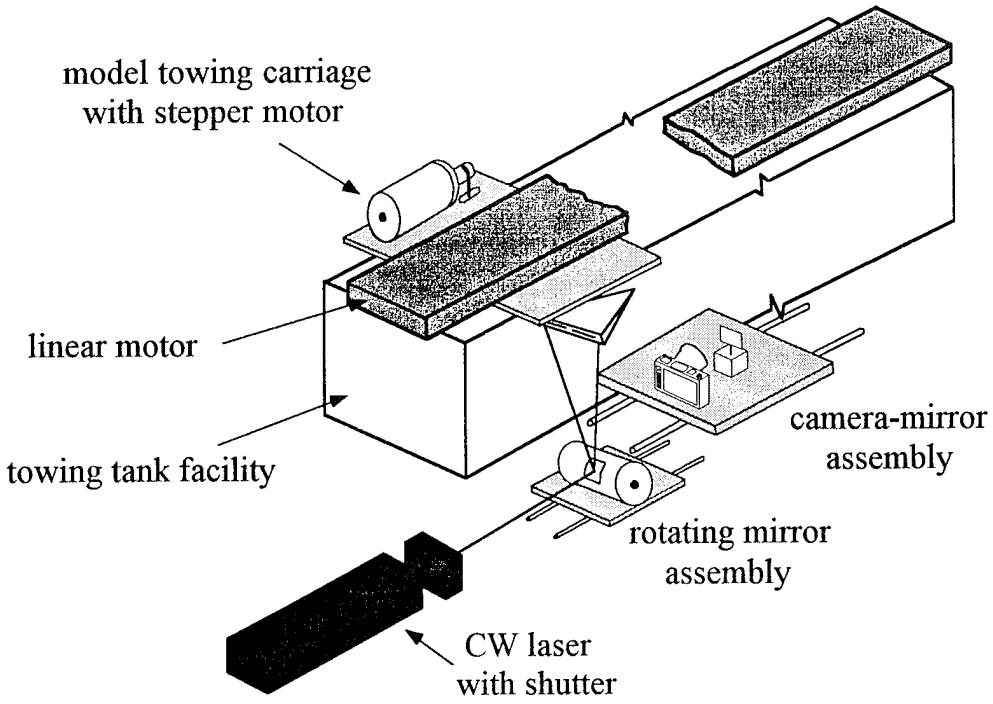

Figure 1 Water towing tank facility and PIV photographic arrangements

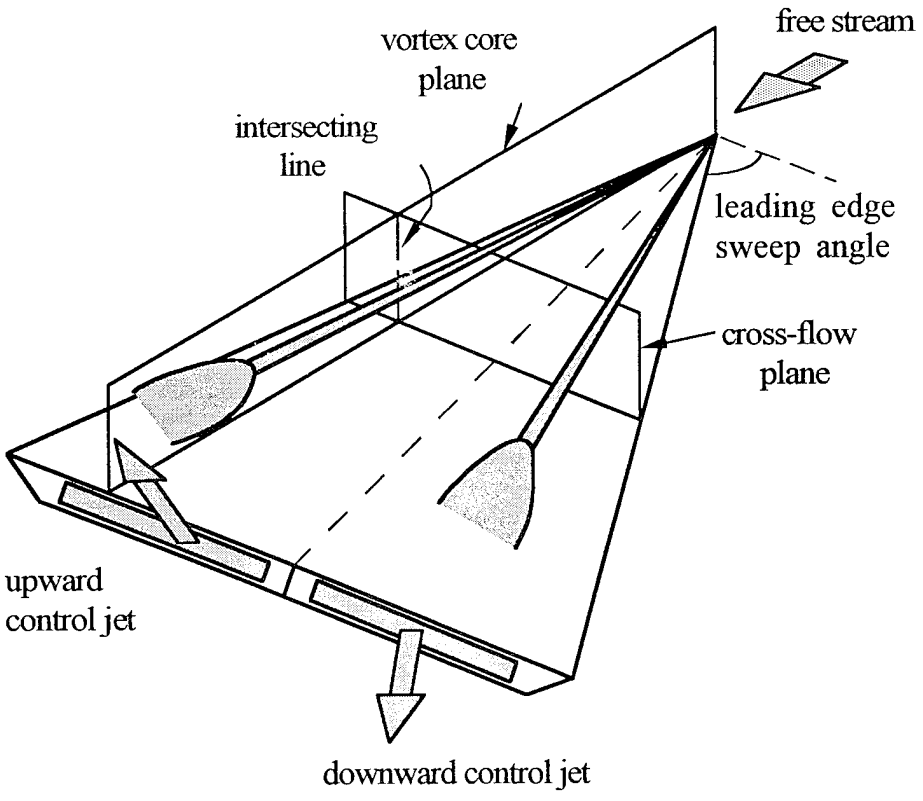

Figure 2 Configuration of the delta wing

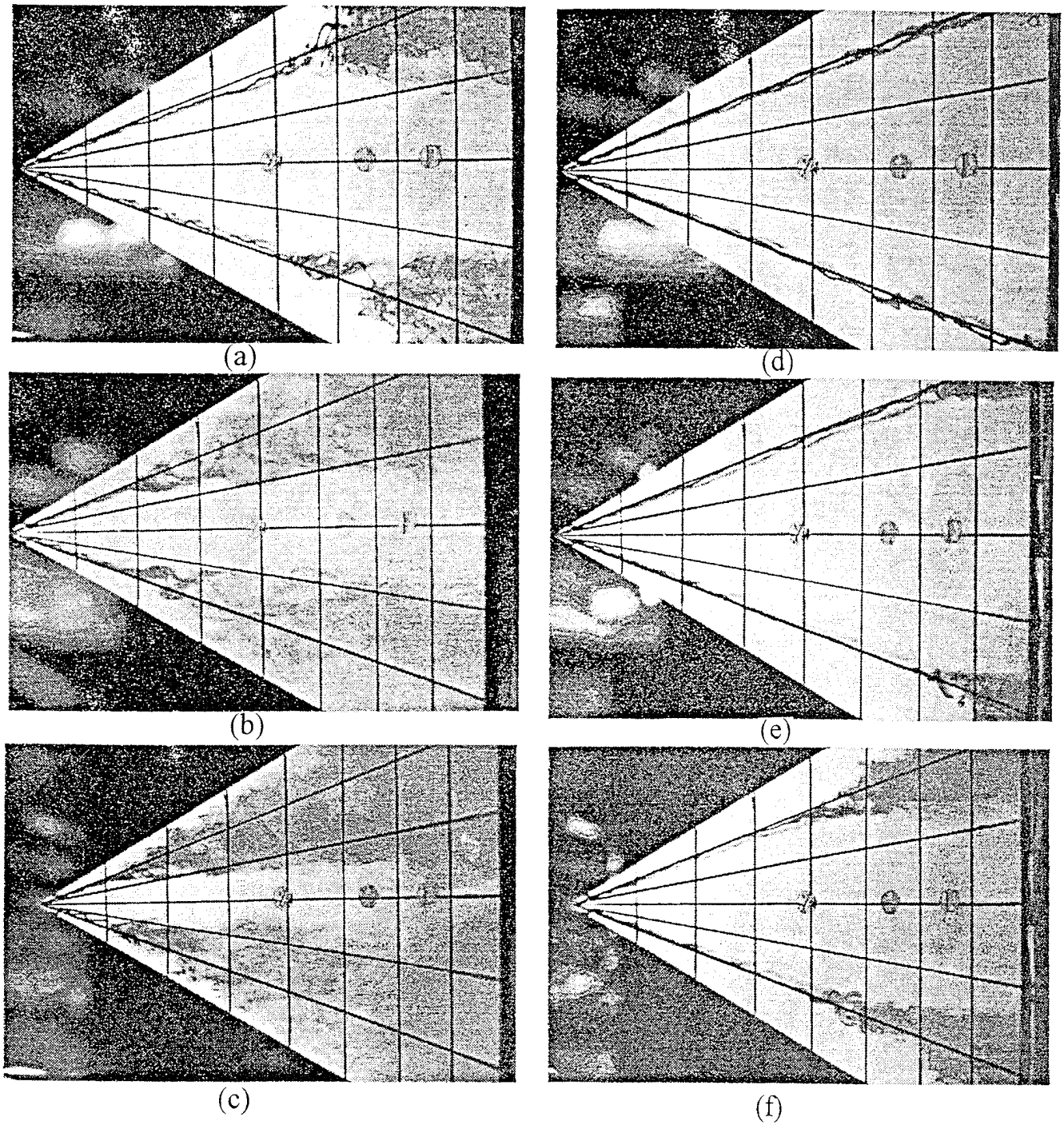

Figure 3 Flow visualization results of a static delta wing.
no control: (a) α=15°, (b) α=20°, (c) α=25°
with control: (d) α=15°, (e) α=20°, (f) α=25°

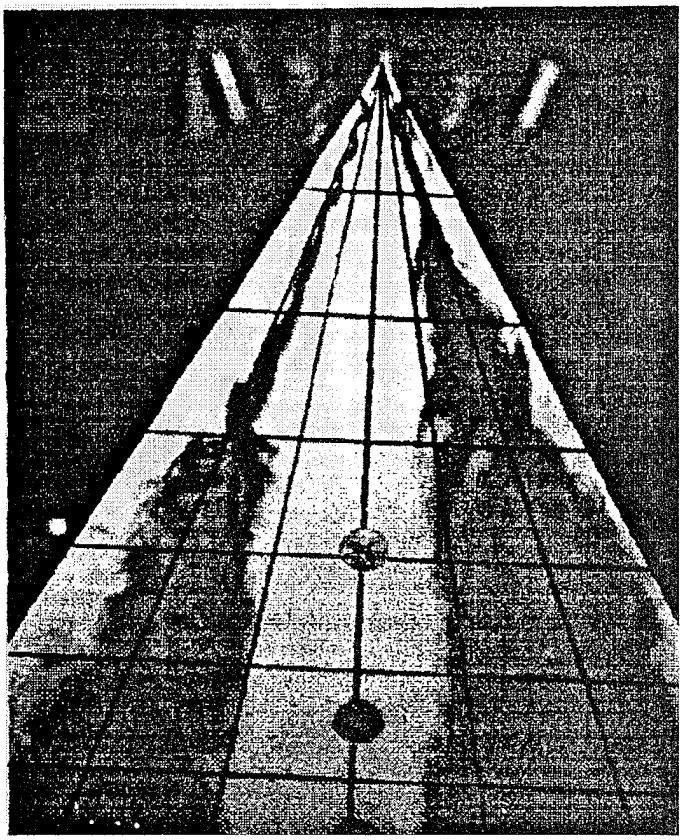

(a)

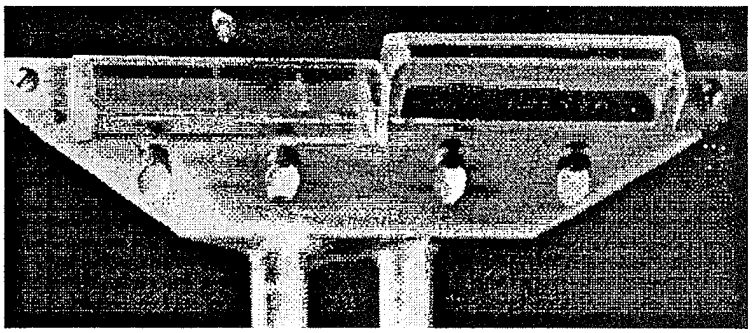

(b)

Figure 4 Asymmetric trailing edge jet control. Left-side jet: 30° downward, right-side jet: 30° upward. (a) flow visualization result of a static delta wing, AOA = 25°, (b) trailing edge nozzle configuration.

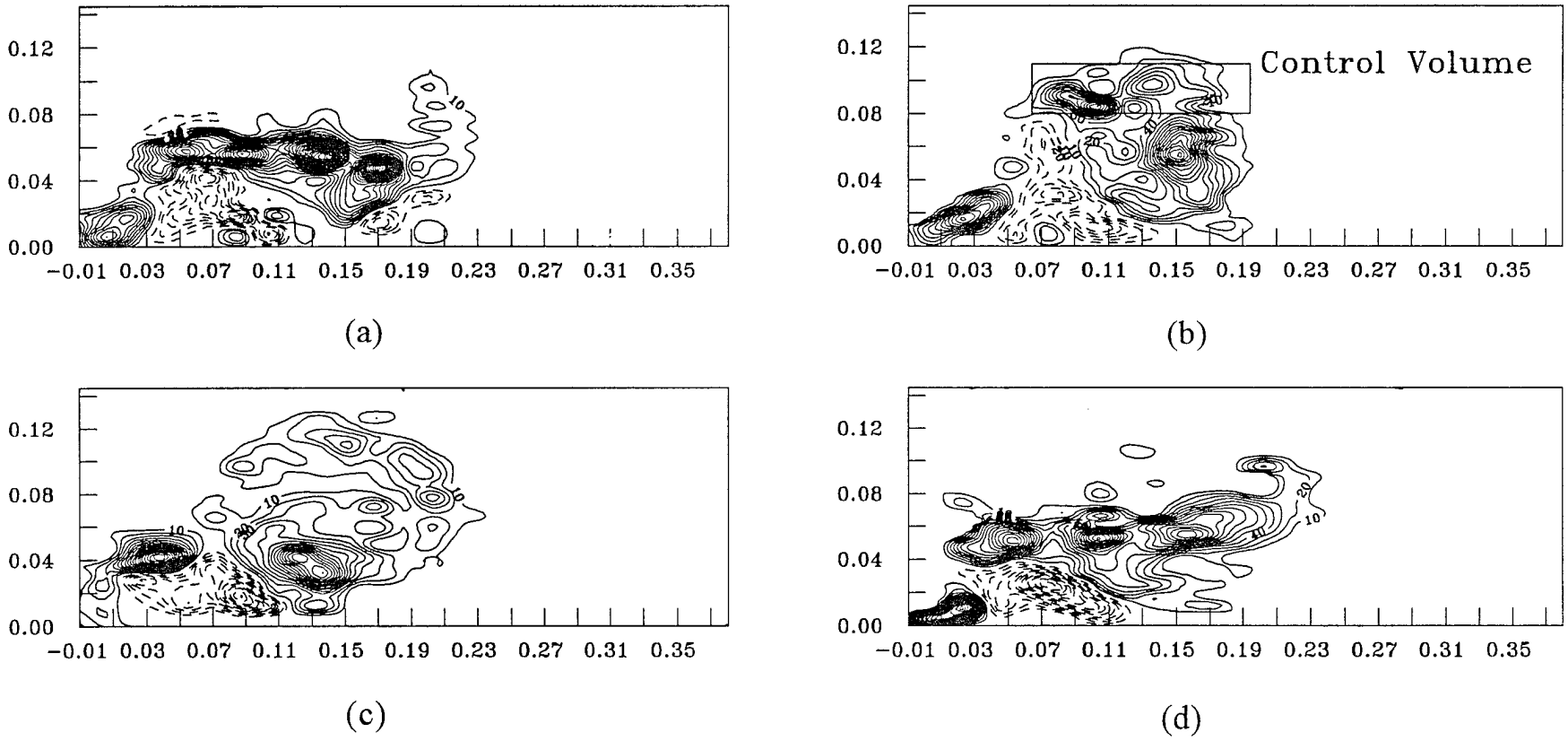

Figure 5 Variation of the instantaneous vortical structures at the cross section of 50% chord, AOA = 12.5°

(a) t^+=0.0, (b) t^+=0.10, (c) t^+=0.19, (d) t^+=0.29

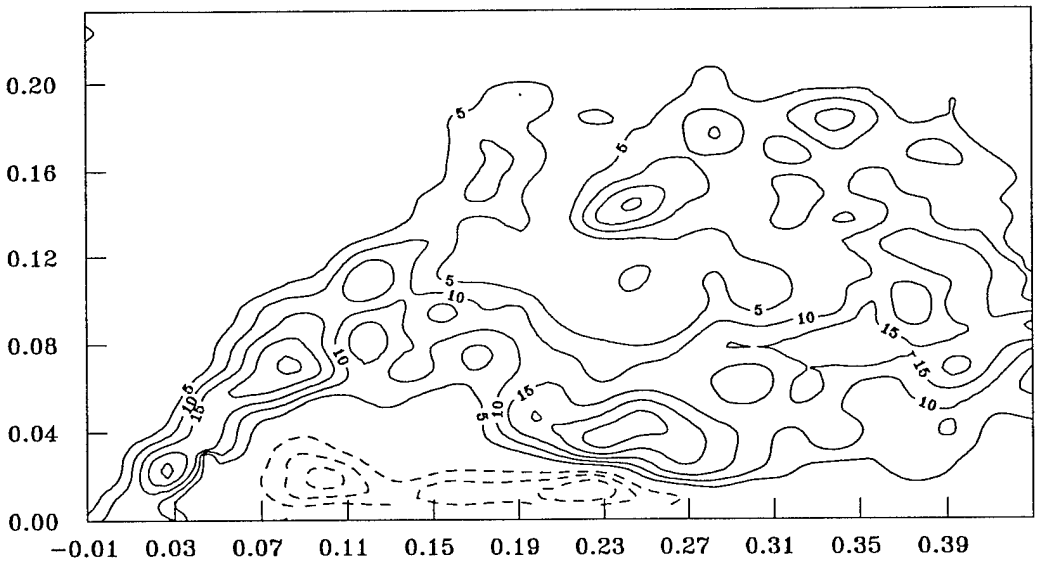

(a)

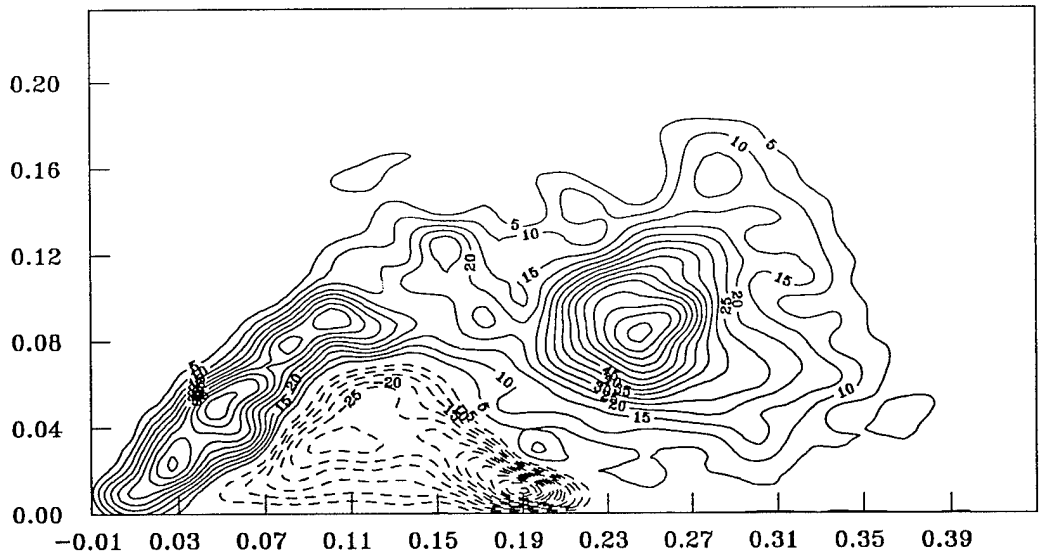

(b)

Figure 6 Averaged vorticity fields at the cross section of 92% chord, AOA = 12.5°. (a) no control (b) with control

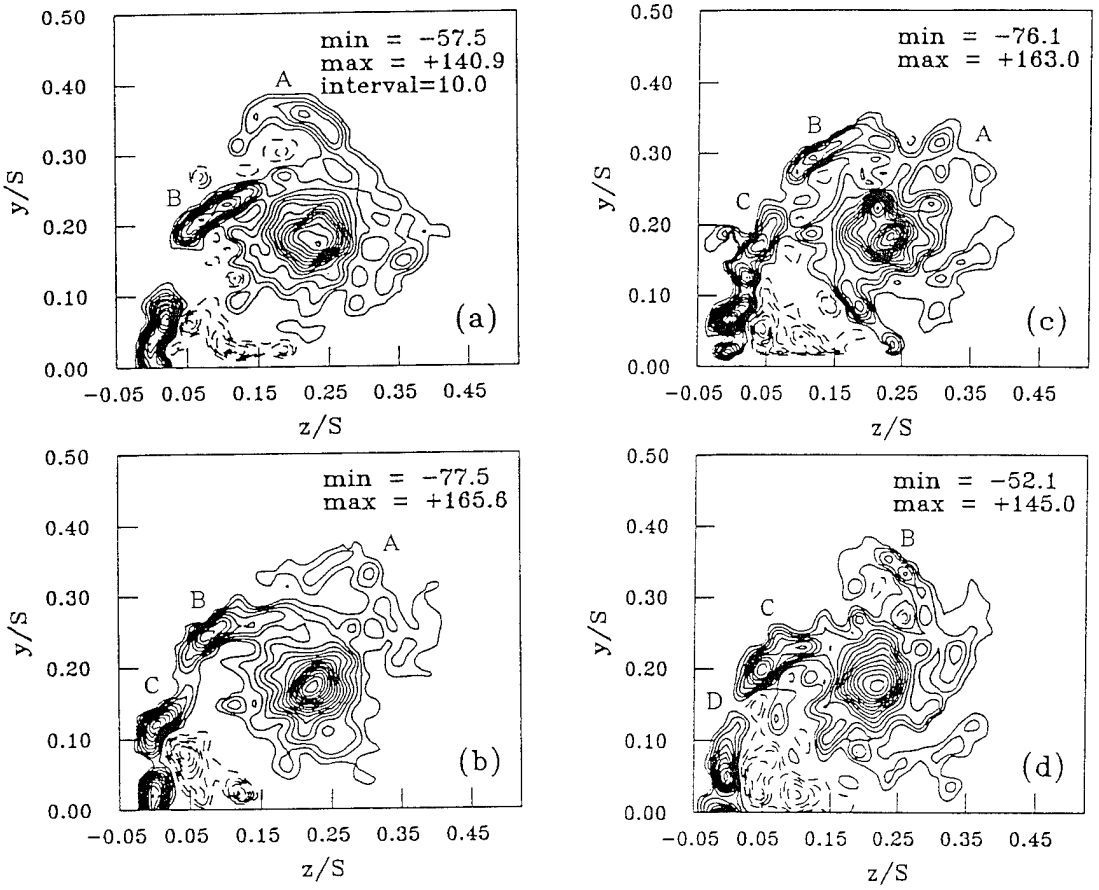

Figure 7 Variation of instantaneous cross-stream vorticity fields at 75% chord. AOA=27.5°. (a) t^+=0.0 (b) t^+=0.07, (c) t^+= 0.15, (d) t^+=0.23

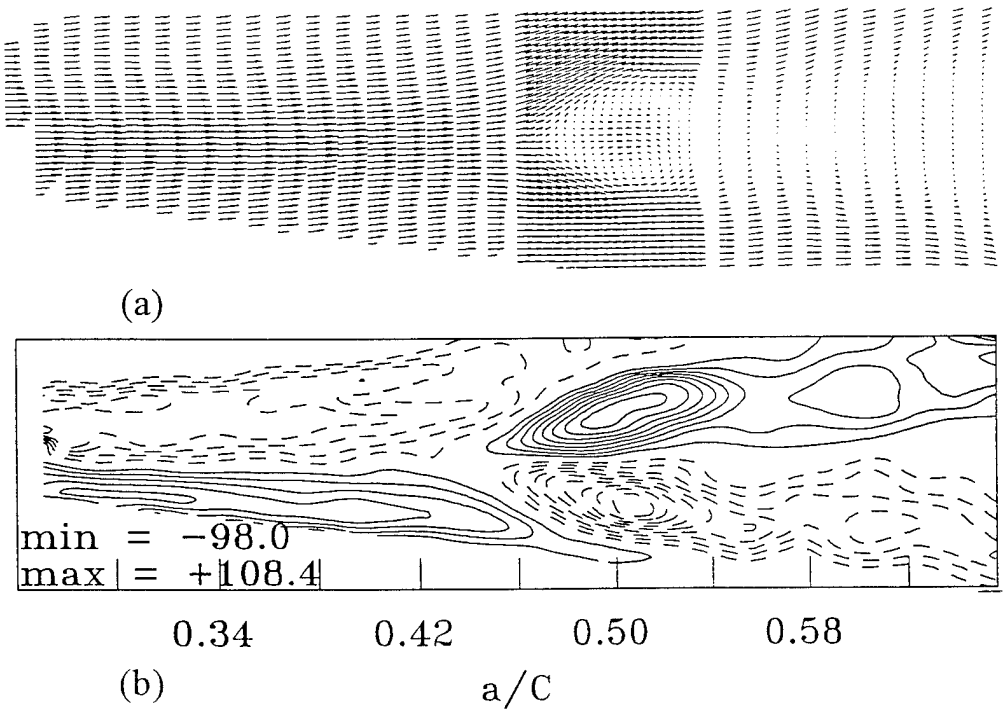

Figure 8 Time averaged (a) velocity and (b) vorticity fields measured along the vortex core axis. AOA=27.5°

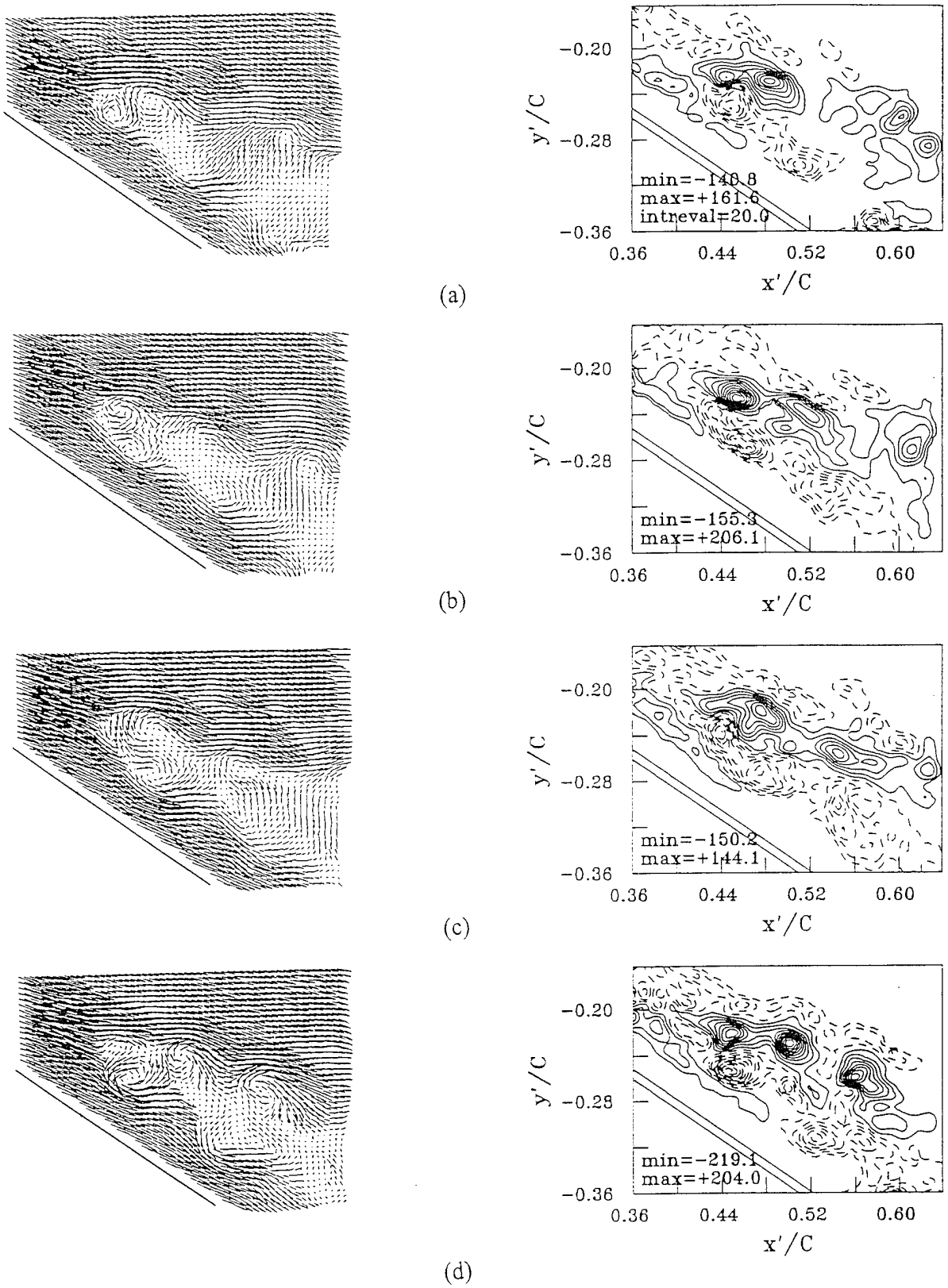

Figure 9 Instantaneous velocity and corresponding vorticity fileds along the vortex core plane. AOA=35°. (a) t^{-}=0.0, (b) t^{-}=0.05, (c)t^{-}=0.11, (d) t^{-}=0.16.